Elemental Enriched Spaces for the Treatment of Weak and Strong Discontinuous Fields

Sergio R. Idelsohn[a,b,*], Juan M. Gimenez[d,e], Julio Marti[b,c], Norberto M. Nigro[d,e]

[a] *Institució Catalana de Recerca i Estudis Avançats (ICREA), Barcelona, Spain*
[b] *Centre Internacional de Mètodes Numèrics en Enginyeria (CIMNE), Barcelona, Spain*
[c] *Universitat Politècnica de Catalunya (UPC), Barcelona, Spain*
[d] *Centro de Investigación de Métodos Computacionales (CIMEC-UNL-CONICET), Santa Fe, Argentina*
[e] *Facultad de Ingeniería y Ciencias Hídricas, Universidad Nacional del Litoral, Santa Fe, Argentina*

Abstract

This paper presents a finite element that incorporate weak, strong and both weak plus strong discontinuities with linear interpolations of the unknown jumps for the modeling of internal interfaces. The new enriched space is built by subdividing each triangular or tetrahedral element in several standard linear sub-elements. The new degrees of freedom coming from the assembly of the sub-elements can be eliminated by static condensation at the element level, resulting in two main advantages: first, an elemental enrichment instead of a nodal one, which present an important reduction of the computing time when the internal interface is moving all around the domain and second, an efficient implementation involving minor modifications allowing to reuse existing finite element codes. The equations for the internal interface are constructed by imposing the local equilibrium between the stresses in the bulk of the element and the tractions driving the cohesive law, with the proper equilibrium operators to account for the linear kinematics of the discontinuity. To improve the continuity of the unknowns on both sides of the elements on which a static condensation is done, a contour integral has been added. These contour integrals named inter-elemental forces can be interpreted as a "do nothing" boundary condition [1] published in another context, or as the usage of weighting functions that ensure convergence of the approach as proposed by J.C. Simo [2]. A series of numerical tests for scalar unknowns as a simple representation of more general numerical simulations are presented to illustrate the performance of the enriched elemental space.

Keywords: Enriched FE spaces, Internal interfaces, Discontinuous fields, Multi-materials, EFEM, Cracks.

1. Introduction

The simultaneous existence of multiple materials with varying physical properties are frequently found in daily life and industrial processes, among many other practical situations. These types of problems are labeled "multi-materials" and they typically exist in different forms depending on the given phase distribution. Examples are gas-liquid transport, magma chambers, fluid-fuel interactions, crude oil recovery, spray cans, sediment transport in rivers and floods, pollutant transport in the atmosphere, cloud formation, fuel injection in engines, bubble column reactors and spray dryers for food processing, to name only a few. This demonstrates the great incidence and also the importance of multi-material problems, which probably occur even more frequently than single materials [3]. As a result of the interaction between the different components, multi-materials are rather complex and very difficult to describe theoretically. The design and optimization of multi-material systems therefore requires a deep understanding of the interface transport phenomena. Furthermore, internal moving sharp gradients or discontinuities in the unknown function in homogeneous materials are also problems that need a special treatment similar to the internal interfaces

*Corresponding author
Email address: sergio@cimne.upc.edu (Sergio R. Idelsohn)

of the multi-material problems. This is for instance the case of crack propagation problems in solids; welding or phase-change in thermal problems; shock waves in compressible flows, among others.

Physical modeling in ad-hoc laboratory scale models is not suitable for this purpose because of its complexity, the difficulty for scaling up to real life problems, its large execution times involved, and hence unaffordable costs and risks. The alternative is nowadays, numerical modeling. For homogeneous flows, computational fluid dynamics (CFD) has already a long history and it is standard a practice to use commercially available CFD codes for the design of, for instance, airplanes and cars. However, because of the complex physics involved in multi-fluid flows the application of CFD in this area is rather young (probably 20-30 years). Despite the practical importance of the problem and the intensive work carried out in the last decade for the development of suitable mathematical and computational models, it is widely accepted that the numerical study of heterogeneous flows is still a major challenge [3]. Different reasons exist for this fact; some are connected to the complex mathematical structure of the multi-fluid problem, others are related to the multi-scale features of the flow. For instance, the presence of breaking waves in a free surface, the existence of one or multiple internal interfaces and, in general, the high unsteadiness of the flow, constitute major obstacles for the analysis. Adding to this the need to reproduce the interaction of free-surface flows with structures as it occurs in many practical problems, may be clearly understood as the reason of why multi-fluid flow problems represent nowadays one of the great challenges in computational engineering science.

In the case of multi-materials, the dynamics of the interface between fluids plays a dominant role. The computation of the interface between various immiscible fluids or the free surfaces is extremely difficult because neither the shape nor the positions of the interfaces are a priori known. The approaches to solve these problems are mainly two: one is based on using a moving mesh that follows the discontinuity, named interface-tracking methods, and the second based on using a fixed mesh refined in that part of the domain where the interface cross during the evaluation named interface-captuting methods. The former computes the motion of the flow particles via a Lagrangian approach where the computational domain adapts itself to the shape and position of the interfaces (see e.g., [4, 5, 6, 7, 8, 9]). A different approach for the simulation of free-surface flows that is based on Lagrangian particles can be found in [10, 11, 12, 13].

In the interface-capturing method (see [14, 15, 16]), the interface is represented by a surface mesh advected with a Lagrangian method while immersed in an Eulerian (fix) mesh where the flow problem is solved considering the fluids as a single effective fluid with variable properties. Popular methods of this type are the volume-of-fluid technique (see [17, 18, 19]) and the level set method (see, for example, [20, 21, 22, 23]). In this case, the flow problem is also solved in a fixed underlying mesh considering a single fluid with variable properties. Variants of these methods mainly differ in two aspects: first, the technique used to solve the transport equation for the scalar function where the interface is embedded, for which a great deal of work has been carried out to improve the accuracy for purely Eulerian methods [24, 25, 26, 27, 28, 29] and for semi-Lagrangian methods [30, 31, 32]. Second, the technique used to solve the Navier-Stokes equations for a one-phase flow with variable properties and in how the fluid-dynamics variables are treated near the interface because these can exhibit discontinuities in their values and/or their gradients owing to the discontinuities in the physical properties and/or the presence of singular forces.Several remedies have been proposed to improve accuracy and robustness of computations in Eulerian formulations. For instance, in Brackbill et al. [33], a treatment of the singular forces at the interface by means of a regularization is proposed, such that sharp variations in the pressure field are avoided. In Löhner et al. [34] and Carrica et al. [35], different extrapolation techniques of the velocity and pressure near the interface are presented.

The finite element solution, either continuous or discontinuous across inter-element boundaries, for such problems when the interface does not necessarily conform to the element edges (in 2D) or faces (in 3D), suffer of sub-optimal approximation orders. This poor approximation leads to spurious velocities near the interface that may significantly affect the precision and the robustness of numerical simulations (see e.g., [36]). A number of methods have been developed to overcome these difficulties. One possibility is to locally modify the finite element spaces in those elements cut by the interface to accommodate the discontinuities. This can be carried out without introducing additional degrees of freedom, using the pressure space proposed by Ausas et al. [37].The interpolation properties of this space are discussed in detail in [38]. The other possibility that is explored in this article is to add degrees of freedom or enrich the finite element space at the elements cut by the interface. Minev et al. [39], and later Chessa and Belytschko [40], adopted an enrichment technique nowadays called XFEM, a name coined in the context of fracture mechanics [41] or named also GFEM by other authors [42, 43]. Both approaches lead to optimal orders of convergence, but the main drawback is that the additional degrees of freedom cannot be eliminated before assembly. The XFEM approach has also been used recently in two-phase flows [44, 45, 46]. These kinds of enrichment have been also called global

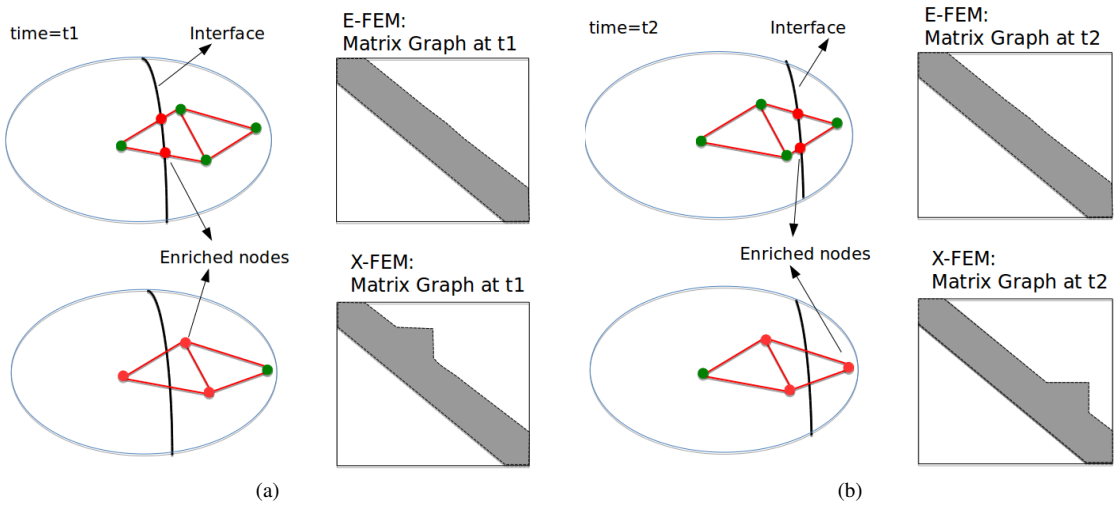

Fig. 1: Matrix-graph when moving the interface. Upper: Elemental enrichment; Bottom: Nodal enrichment. (a) Before movement. (b) After movement

enrichment or nodal enrichment, or as stated before XFEM or GFEM. A method that avoids the inclusion of additional degrees of freedom is that one presented by Fries et al. [47], which, on the other hand, has the drawback of using second-neighbor connectivities arising from the moving least square approach that it uses. Also, in [48], Codina and Coppola-Owen introduced an enrichment for the treatment of kinks in the pressure field as typically happens in problems with jumps in the density in the presence of a gravitational field. This strategy allows to statically condense the additional degree of freedom prior to the assembly, as deeply explained by [49]. For this reason, these kinds of enrichment have been named elemental enrichment or EFEM. A generalization of the treatment of kinks and jumps in the pressure field was presented by Idelsohn et. al. in [50]. However, the enriched space proposed in [50] works satisfactorily for the pressure field in the Navier-Stokes equations but does not work correctly for the enrichment of the temperature field in a typical thermal problem or for the enrichment of the displacement or the velocity field in solid or fluid mechanics problems. The advantages of the EFEM compared with the global enrichment GFEM is the huge reduction of the computing time when the internal interface is moving. In the EFEM the matrix to be solved at each time-step has, not only the same amount of degrees of freedom (DOFs) but also has always the same connectivity between the DOFs. This means that the matrix-graph remains constant while in the GFEM the matrix-graph is permanently changing (see Figure 1). This frozen graph improves enormously the efficiency of the solver, mainly in 3D problems [51, 52]. The disadvantage of the EFEM is the impossibility to be exactly consistent with the internal continuities required for the variational form. The way to mitigate these inconsistencies (also called variational crimes) is one of the main target of this work.

In this work a fixed mesh method with a new enrichment technique is proposed. The corresponding enriched finite element space is suitable for treating different kinds of interface discontinuities such as jumps (discontinuity of the unknown field) or kinks (discontinuity of the gradient of the unknown field). The new enriched space decreases considerably the variational crimes introduced when an elemental enrichment is used for unknown fields that are under second order derivatives in space, like displacements, velocities and temperature in the conservation equations.Another characteristic of the new elemental enriched space is that allows a linear variation of the jump, improving the convergence rate to the exact solution compared with other enriched spaces that have a constant variation of the jump. This linear variation was previously proposed in [53] but only for quadrangles in a solid mechanics context. The implementation in any existing finite element code is extremely easy in both two and three spatial dimensions, because the new shape functions are based on the usual C^0 FEM shape functions for triangles or tetrahedral and, once statically condensed the internal DOFs, the resulting elements have exactly the same number of unknowns as the non-enriched FE. To show the accuracy of the new space proposed, simple but very convincing examples are presented as numerical examples.

The remainder of the paper is organized as follows. In the next section, we present the governing equation, and the corresponding discrete formulation. In the following section, we introduce the enrichment functions used and explain its formulation for solving the model problem with three-node triangular elements. Also, special considerations are discussed. It must be noted that the application of the new enrichment is not limited to the convection-diffusion equation and can be easily applied to other problems (such as structural problems) with strong and weak discontinuities. Finally some numerical results are presented and compared with other conventional formulations. A detailed convergence study for this method is provided in the results section by comparing it with the standard FEM.

2. The governing equations

In this work typical steady conservation equations, like those used in the energy conservation in heat conduction problems or those used in the momentum conservation equations in solid and fluid mechanics problems, will be numerically solved using an enriched space. The idea is to introduce the enriched space in those equations in which the unknown appears as a second derivative in space. This means that an integration by parts is needed in order to solve this equation in a Finite Element context.

In fact, for simplicity reasons, the examples will be presented only for the scalar heat conduction problem. Nevertheless, the reader may take into account that the ideas presented herein may be used in many other applications, in particular in the context of solid mechanics for the case of discontinuous displacement like those existing in crack problems or in the context of fluid mechanics for the case of discontinuities in the pressure, the pressure gradients, the velocities and the velocity gradients, due to the presence of multi-fluids and or multi-phase flows.

The steady conservation equations in a general way will be written as:

$$\nabla \cdot \boldsymbol{\sigma} + \mathbf{b} = \mathbf{0} \tag{1}$$

where $\boldsymbol{\sigma}(\mathbf{x})$ represents the stress tensor (or the heat fluxes for a thermal problem), and $\mathbf{b}(\mathbf{x})$ a vector source term (scalar source for a thermal problem). The stresses (or the fluxes) are related to the strain (temperature gradient) through the constitutive equations:

$$\boldsymbol{\sigma} = \mathbf{C} : \boldsymbol{\epsilon} \tag{2}$$

where $\mathbf{C}$ is the fourth order tensor of physical material coefficients and $\boldsymbol{\epsilon}$ the strain tensor defined in terms of the unknown field $\mathbf{u}$:

$$\boldsymbol{\epsilon} = \nabla^S \mathbf{u} \tag{3}$$

This unknown field may be the displacement vector for the case of solid mechanics problems, the velocity vector for the case of fluid mechanics problems, the scalar temperature for the case of thermal energy conservation, the pressure field or any other unknown variable related by equations of the type of (1-3). The symbol ∇^S is the symmetric gradient of the unknown, in this case applied on the displacement vector field and defined as:

$$(\nabla^S \mathbf{u})_{ij} = \frac{1}{2}\left(\frac{\partial u_i}{\partial x_j} + \frac{\partial u_j}{\partial x_i}\right) \tag{4}$$

producing as a result a tensor field, or simply the gradient for the scalar unknown as:

$$(\nabla^S u)_i = (\nabla u)_i = \frac{\partial u}{\partial x_i} \tag{5}$$

producing a vector field. The possible boundary conditions for the typical conservation equation 1 are:

$$\overline{\boldsymbol{\sigma}_n} = \boldsymbol{\sigma}_n = \mathbf{C} : (\nabla^S \mathbf{u}) \cdot \mathbf{n} \qquad \text{on } \Gamma_\sigma \tag{6}$$

and

$$\overline{\mathbf{u}} = \mathbf{u} \qquad \text{on } \Gamma_{\mathbf{u}} \tag{7}$$

where $\overline{\boldsymbol{\sigma}_n}$ and $\overline{\mathbf{u}}$ represent imposed values of the normal fluxes (stresses or heat fluxes) and the unknown (displacements, velocities or temperature) respectively and $\mathbf{n}$ the outside normal vector.

Possible internal conditions at the interfaces may be of two types:

- (a) Kinks:

$$\boldsymbol{\sigma}_n^+ + \boldsymbol{\sigma}_n^- = \overline{\boldsymbol{\sigma}_n^{\text{int}}} \qquad \text{on } \Gamma_{\text{int}} \tag{8}$$

- (b) Jumps:

$$\begin{cases} \boldsymbol{\sigma}_n^+ - \overline{\boldsymbol{\sigma}_n^{+\,\text{int}}} = \mathbf{J} \parallel \mathbf{u} \parallel^+ = \mathbf{J}(\mathbf{u}_n^- - \mathbf{u}_n^+) \\ \boldsymbol{\sigma}_n^- - \overline{\boldsymbol{\sigma}_n^{-\,\text{int}}} = \mathbf{J} \parallel \mathbf{u} \parallel^- = \mathbf{J}(\mathbf{u}_n^+ - \mathbf{u}_n^-) \end{cases} \qquad \text{on } \Gamma_{\text{int}} \tag{9}$$

where $\overline{\boldsymbol{\sigma}_n^{\text{int}}}$ is a known normal stress imposed on the interface Γ_{int} ; $\boldsymbol{\sigma}_n^+$ and $\boldsymbol{\sigma}_n^-$ the normal stresses on both sides of the interface considering positive in the sense of the outside unit normal to the interface respectively and $\parallel \mathbf{u} \parallel^+ = (\mathbf{u}_n^- - \mathbf{u}_n^+)$ the unknown jump on both sides of the interface in a coordinate parallel to the outside normal vector. Finally $\mathbf{J}$ plays the role of the tensor ($\mathbf{C}$:) in 2, that means, 9 is a constitutive equation between the jump unknown and the stresses. In what follow, a constant $\mathbf{J}$ tensor will be considered but any other non-linear relation $\mathbf{J} = \mathbf{J}(\parallel \mathbf{u} \parallel)$ may be introduced. For the case of thermal problem, $\mathbf{J}$ is a scalar representing the amount of thermal flux going through the contact between two bodies proportional to the jump in the temperature field at each sides. Extensions to another more complicated constitutive equation may be used without changing the enriched space to be used in this paper.

As Finite Element Method (FEM) will be used as numerical method to solve equations 1 to 9, internal compatibilities and equilibrium at the interface between two elements where the FEM introduces artificial kinks in the unknown functions must be added. They are expressed as:

$$\begin{cases} \boldsymbol{\sigma}_n^+ + \boldsymbol{\sigma}_n^- = 0 \\ \mathbf{u}_n^- = \mathbf{u}_n^+ \end{cases} \qquad \text{on } \Gamma_{\text{l}} \tag{10}$$

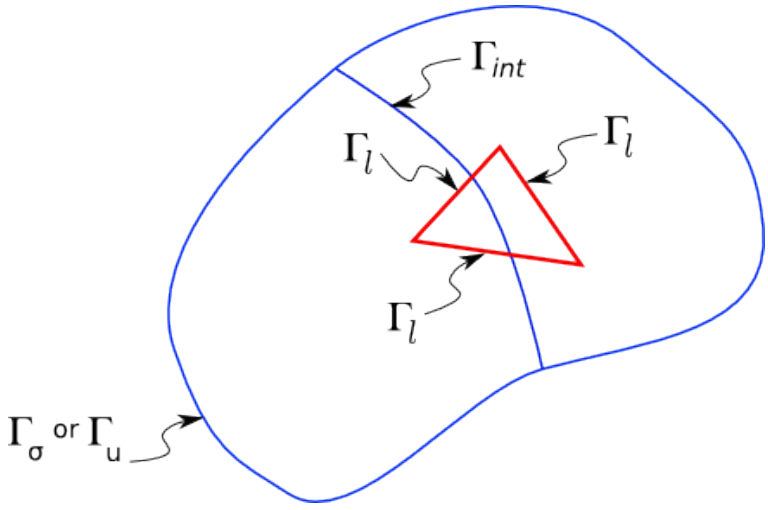

Fig. 2: Interface names

where Γ_{l} is considered as the whole boundary of the finite element l, and + and − represent both sides of the inter-element interfaces. The imposition of the conditions 10 is normally intrinsic to the variational form of the equations

used to solve a problem using the FEM. However, they take special relevance when using discontinuous enriched spaces as those that will be used in this work.

3. Variational formulation of the governing equations: the weighted residual form

The weighted residual form of Eq. 1 with the boundary conditions 6 and the internal conditions for kinks 8 reads:

$$\int_{\Omega} \mathbf{w} \cdot [\nabla \cdot (\mathbf{C} : \nabla^S \mathbf{u}) + \mathbf{b}] d\Omega + \int_{\Gamma_\sigma} \mathbf{w} \cdot (\overline{\boldsymbol{\sigma}_n} - \boldsymbol{\sigma}_n) d\Gamma + \int_{\Gamma_{\text{int}}} \mathbf{w} \cdot (\overline{\boldsymbol{\sigma}_n^{\text{int}}} - \boldsymbol{\sigma}_n^+ - \boldsymbol{\sigma}_n^-) d\Gamma = 0 \tag{11}$$

where $\mathbf{w}$ is any continuous weighting function satisfying that $\mathbf{w} = 0$ on Γ_u.

For the case of FEM, where the unknown functions $\mathbf{u}$ as well as the weighting functions $\mathbf{w}$ belong to the C^0 space, this means continuous functions but with discontinuous derivative between two neighbor elements, the integral on the total domain must be subdivided into a sum of integrals on each element where the functions to be integrated by parts are continuous. In this case, the condition 10 must be added to the weighted form to ensure the continuity of the normal stresses:

$$\begin{aligned} \sum_{l=1}^{\text{Ne}} \Big\{ \int_{\Omega_l} \mathbf{w} \cdot [\nabla \cdot (\mathbf{C} : \nabla^S \mathbf{u}) + \mathbf{b}] d\Omega + \int_{\Gamma_\sigma \cap \Gamma_l} \mathbf{w} \cdot (\overline{\boldsymbol{\sigma}_n} - \boldsymbol{\sigma}_n) d\Gamma + \int_{\Gamma_{\text{int}} \cap \Omega_l} \mathbf{w} \cdot (\overline{\boldsymbol{\sigma}_n^{\text{int}}} - \boldsymbol{\sigma}_n^+ - \boldsymbol{\sigma}_n^-) d\Gamma \Big\} + \\ \cdots - \sum_{l=1}^{\text{Ne}} \Big\{ \int_{\Gamma_l} \mathbf{w} \cdot (\boldsymbol{\sigma}_n^+ + \boldsymbol{\sigma}_n^-) d\Gamma \Big\} = 0 \end{aligned} \tag{12}$$

In Eq. 12 the super index $(\pm)$ on the stresses means the stress on the neighbor elements. Integrating by parts the first term of Eq. 12, the standard variational form of the momentum equation is obtained:

$$\sum_{l=1}^{\text{Ne}} \Big\{ \int_{\Omega_l} [-\nabla^S \mathbf{w} : (\mathbf{C} : \nabla^S \mathbf{u}) + \mathbf{w} \cdot \mathbf{b}] d\Omega + \int_{\Gamma_\sigma \cap \Gamma_l} \mathbf{w} \cdot \overline{\boldsymbol{\sigma}_n} d\Gamma + \int_{\Gamma_{\text{int}} \cap \Omega_l} \mathbf{w} \cdot \overline{\boldsymbol{\sigma}_n^{\text{int}}} d\Gamma \Big\} = 0 \tag{13}$$

It must be noted that in Eq.13 the condition imposed by Eq. 10 disappears in the variational form after integration by parts. This happens because the standard weighting functions are continuous between two neighbor elements.

4. Variational formulation of the elemental enrichment

In the FEM the unknown functions are approximated by the standard FE shape functions:

$$\mathbf{u}(\mathbf{x}) = \sum_{l=1}^{\text{Nn}} \mathbf{N}_l(\mathbf{x}) \mathbf{a}_l = \mathbf{N}^T \mathbf{a} \tag{14}$$

where $\mathbf{a}_l$ are the local values of the unknown $\mathbf{u}$ at the node l and $\mathbf{N}_l(\mathbf{x})$ are the standard shape functions that are of unit value on the node l and of zero value on the other nodes belonging to the element being treated, as usually.

To enrich a FE space means to add some new shape functions that are activated in some cases and deactivated in other ones. Here, the new shape functions must be able to reproduce the discontinuity sought inside some elements. Let's write:

$$\mathbf{u}(\mathbf{x}) = \mathbf{N}^T \mathbf{a} + (\mathbf{N}^e)^T \mathbf{a}^e \tag{15}$$

where the enriched shape functions $\mathbf{N}^e(\mathbf{x})$ must be able to represent a kink or a jump inside each element.

The main difference between the global enrichment (GFEM) and the local or elemental enrichment (EFEM) is that in the first one, the $\mathbf{N}^e(\mathbf{x})$ shape functions are defined at the nodal level while in the EFEM they are defined inside the elements.

In the elemental enrichment the enriched part of the shape functions may present discontinuities between one element and its neighbor. The same happens with the weighting functions when a Galerkin approximation is used ($\mathbf{w}^e = \mathbf{N}^e$). In this context, $\mathbf{N}$ are the standard (nodal) shape functions while $\mathbf{w}$ are the standard weighting functions. The super index e is used for both the shape function enriched space and the corresponding weighting function enriched.

The weighted residual form 12 for the enriched part of the weighting functions remains:

$$\sum_{l=1}^{\text{Ne}} \Big\{ \int_{\Omega_l} \mathbf{w}^e \cdot [\nabla \cdot (\mathbf{C} : \nabla^S \mathbf{u}) + \mathbf{b}] d\Omega + \int_{\Gamma_\sigma \cap \Gamma_l} \mathbf{w}^e \cdot (\overline{\boldsymbol{\sigma}_n} - \boldsymbol{\sigma}_n) d\Gamma + \int_{\Gamma_{\text{int}} \cap \Omega_l} \mathbf{w}^e \cdot (\overline{\boldsymbol{\sigma}_n^{\text{int}}} - \boldsymbol{\sigma}_n^+ - \boldsymbol{\sigma}_n^-) d\Gamma \Big\} + \cdots - \sum_{l=1}^{\text{Ne}} \Big\{ \int_{\Gamma_l} \mathbf{w}^e \cdot (\boldsymbol{\sigma}_n^+ + \boldsymbol{\sigma}_n^-) d\Gamma \Big\} = 0 \tag{16}$$

and integrating by parts, the variational form of the enriched space is obtained:

$$\sum_{l=1}^{\text{Ne}} \Big\{ \int_{\Omega_l} \Big[-\nabla^S \mathbf{w}^e : (\mathbf{C} : \nabla^S \mathbf{u}) + \mathbf{w}^e \cdot \mathbf{b} \Big] \, d\Omega + \int_{\Gamma_\sigma \cap \Gamma_l} \mathbf{w}^e \cdot \overline{\boldsymbol{\sigma}_n} \, d\Gamma + \int_{\Gamma_{\text{int}} \cap \Omega_l} \mathbf{w}^e \cdot \overline{\boldsymbol{\sigma}_n^{\text{int}}} \, d\Gamma \Big\} - \sum_{l=1}^{\text{Ne}} \int_{\Gamma_l} \mathbf{w}^e \cdot \boldsymbol{\sigma}_n^+ \, d\Gamma = 0 \tag{17}$$

It must be noted that the last term of the second equation 17 so does not disappear as in 13 because the functions $\mathbf{w}^e$ are defined only inside each element.

The stresses $\boldsymbol{\sigma}_n^+$ correspond to the normal stresses in the neighbor element. This means that in order to fulfill the correct equilibrium equation expressed in 10 the stresses in the neighbor elements are needed.

Many authors avoid directly the last term of 17 [51, 52]. This means to impose the normal stresses to be zero on the boundaries of each enriched element. Although this satisfies the variational principle the imposition of a zero normal stresses introduces a large error in the results which are not consistent with the physics of the problem. In this work a different approximation is proposed: to evaluate $\boldsymbol{\sigma}_n^+$ on the element boundaries using $\boldsymbol{\sigma}_n^-$, i.e., the normal stresses evaluated at the same element.

$$\sum_{l=1}^{\text{Ne}} \int_{\Gamma_l} \mathbf{w}^e \cdot \boldsymbol{\sigma}_n^+ d\Gamma \approx - \sum_{l=1}^{\text{Ne}} \int_{\Gamma_l} \mathbf{w}^e \cdot \boldsymbol{\sigma}_n^- d\Gamma = - \sum_{l=1}^{\text{Ne}} \int_{\Gamma_l} \mathbf{w}^e \cdot \Big(\mathbf{C} : \nabla^S \mathbf{u} \Big) \cdot \mathbf{n} d\Gamma \tag{18}$$

The integrals in 18 must be evaluated in all the element boundaries where $\mathbf{w}^e \neq 0$. These integrals will be named in the following "inter-element forces" because they are similar to the introduction of a load on both boundaries of two neighbor elements. However, the addition of the integrals 18 to the variational form 13 must not be thought as the addition of a boundary load. It must be better thought as a "do nothing" boundary conditions between the two neighbor elements. In fact, the addition of the integral 18 means to avoid the condition 10 between the two elements.

The "do nothing" boundary condition was first proposed in [54] to improve the outflow boundary condition in unbounded flows. It was later generalized to slip boundary condition in [55] and discussed also in [1]. In this new enriched space, we will use this "do nothing" boundary condition to improve the discontinuity existing between two elements in the case of elemental enrichment. As can be seen in the numerical examples, these inter-element forces improve considerably the accuracy of the elemental enrichment, decreasing (and in many cases eliminating) the artificial jump that appears between two neighbor elements due to the static condensation of the enriched DOF.

Unfortunately, in spite of using a Galerkin approximation, the inter-element forces introduce an asymmetry in the stiffness matrix. Nevertheless, the improvements in the results that are obtained using these forces counteract the disadvantage of asymmetry in the matrices.

The variational form for the enriched space remains:

$$\sum_{l=1}^{\text{Ne}}\Big\{\int_{\Omega_l}[-\nabla^S\mathbf{w}:(\mathbf{C}:\nabla^S(\mathbf{N}^T\mathbf{a}+(\mathbf{N}^e)^T\mathbf{a}^e))+\mathbf{w}\cdot\mathbf{b}]d\Omega+\int_{\Gamma_\sigma\cap\Gamma_l}\mathbf{w}\cdot\overline{\boldsymbol{\sigma}_n}d\Gamma+\int_{\Gamma_{\text{int}}\cap\Omega_l}\mathbf{w}\cdot\overline{\boldsymbol{\sigma}_n^{\text{int}}}d\Gamma\Big\}=0$$

$$\sum_{l=1}^{\text{Ne}}\Big\{\int_{\Omega_l}[-\nabla^S\mathbf{w}^e:(\mathbf{C}:\nabla^S(\mathbf{N}^T\mathbf{a}+(\mathbf{N}^e)^T\mathbf{a}^e))+\mathbf{w}^e\cdot\mathbf{b}]d\Omega+\int_{\Gamma_\sigma\cap\Gamma_l}\mathbf{w}^e\cdot\overline{\boldsymbol{\sigma}_n}d\Gamma+\int_{\Gamma_{\text{int}}\cap\Omega_l}\mathbf{w}^e\cdot\overline{\boldsymbol{\sigma}_n^{\text{int}}}d\Gamma\Big\}- \tag{19}$$

$$\sum_{l=1}^{\text{Ne}}\int_{\Gamma_l}\mathbf{w}^e\cdot(\mathbf{C}:\nabla^S(\mathbf{N}^T\mathbf{a}+(\mathbf{N}^e)^T\mathbf{a}^e))\cdot\mathbf{n}d\Gamma=0$$

With a similar algebra, it is easy to show that for the case of interfaces with kinks + jumps 8,9 the variational form 17 remains:

$$\sum_{l=1}^{\text{Ne}}\Big\{\int_{\Omega_l}[-\nabla^S\mathbf{w}:(\mathbf{C}:\nabla^S\mathbf{u})+\mathbf{w}\cdot\mathbf{b}]d\Omega+\int_{\Gamma_\sigma\cap\Gamma_l}\mathbf{w}\cdot\overline{\boldsymbol{\sigma}_n}d\Gamma+\int_{\Gamma_{\text{int}}\cap\Omega_l}\mathbf{w}\cdot\overline{\boldsymbol{\sigma}_n^{\text{int}}}d\Gamma\Big\}=0$$

$$\sum_{l=1}^{\text{Ne}}\Big\{\int_{\Omega_l}[-\nabla^S\mathbf{w}^e:(\mathbf{C}:\nabla^S\mathbf{u})+\mathbf{w}^e\cdot\mathbf{b}]d\Omega+\int_{\Gamma_\sigma\cap\Gamma_l}\mathbf{w}^e\cdot\overline{\boldsymbol{\sigma}_n}d\Gamma+\cdots+ \tag{20}$$

$$\int_{\Gamma_{\text{int}}\cap\Omega_l}\Big[\mathbf{w}^{e+}\cdot(\overline{\boldsymbol{\sigma}_n^{\text{int}+}}+\mathbf{J}\parallel\mathbf{u}\parallel^+)+\mathbf{w}^{e-}\cdot(\overline{\boldsymbol{\sigma}_n^{\text{int}-}}+\mathbf{J}\parallel\mathbf{u}\parallel^-)\Big]d\Gamma\Big\}-\sum_{l=1}^{\text{Ne}}\int_{\Gamma_l}\mathbf{w}^e\cdot\boldsymbol{\sigma}_n^+d\Gamma=0$$

As in 17 the last term in 20 represents the stresses in the neighbor elements. As in 18, these stresses were replaced by the stresses in the own element as in the previous approximation followed by a "do nothing" boundary condition. The remaining two integrals in the last equation of 20 represent known normal stresses imposed on the interface Γ_{int}. In the case of a jump, these normal stresses may be different from one side to the other side of the interface.

The inter-elemental forces have another very interesting explanation. In [2] the authors show that for some kind of non-conforming linear elements, a condition to guarantee the convergence of the method is to take weighting functions that satisfy the following equation:

$$\int_\Omega\nabla\mathbf{w}d\Omega=0 \tag{21}$$

Furthermore, in the same work ([2]) J.C. Simo et al. proposed and used this condition to satisfy the convergence of an enriched space. They showed that the enriched weighting functions must satisfy the condition

$$\int_\Omega\nabla^S\mathbf{w}^ed\Omega=0 \tag{22}$$

to guarantee convergence of the approximation.

The enriched shape functions proposed in 15 do not necessarily satisfy the restriction 22 and, of coarse, the weighting functions (when a Galerkin approach is used) neither. However, let us consider another enriched weighting function such that $\mathbf{w}^{e*}=\mathbf{w}^e=\mathbf{N}^e$ inside the whole element domain except on the contours, where we assume that $\mathbf{w}^{e*}$ drops to zero abruptly. Under these considerations, it is $\mathbf{w}^{e*}=0$ on the element boundaries, and then 22 is satisfied:

$$\int_\Omega\nabla^S\mathbf{w}^{e*}d\Omega=0 \tag{23}$$

By simple regularization techniques it is easy to show that

$$\int_\Omega\nabla^S\mathbf{w}^{e*}d\Omega=\int_\Omega\nabla^S\mathbf{w}^ed\Omega-\int_\Gamma\mathbf{w}^e\cdot\mathbf{n} \tag{24}$$

Equation 24 means that the use of a Petrov-Galerkin weighting functions likes w^{e*} introduces in a natural way the inter-element forces:

$$\int_\Omega \mathbf{w}^{e*}\nabla^S : (\mathbf{C} : \nabla^S \mathbf{u}) d\Omega = -\int_\Omega \nabla^S \mathbf{w}^{e*} : (\mathbf{C} : \nabla^S \mathbf{u}) d\Omega = -\int_\Omega \nabla^S \mathbf{w}^e : (\mathbf{C} : \nabla^S \mathbf{u}) d\Omega + \int_\Gamma \mathbf{w}^e \cdot (\mathbf{C} : \nabla^S \mathbf{u}) \cdot \mathbf{n} d\Gamma \quad (25)$$

In other words, the inter-element forces may be thought as the results of imposing a "do nothing" boundary condition between two elements, or, as the result of a Petrov-Galerkin approximation with weighting functions that satisfy the convergence criteria 22 proposed by Simo. Both reasons justify, in a different way, the use of the inter-element forces.

5. The enriched space to obtain discontinuous fields and discontinuous gradients fields

The standard way to introduce an enriched space is to add to the FE shape functions as many new shape functions as needed. The remaining set of shape functions do not satisfy the partition of unity condition (PUC), that is, the sum of all the shape functions in any point of the domain is not equal to one. However, to satisfy the PUC has several advantages to evaluate the final unknown and it is easy to show that it is possible to have exactly the same enriched space satisfying the PUC. To this end changing the FE shape functions is needed. Figure 3 shows for instance the one-dimensional FE linear shape functions for one element and the enriched shape function to add a kink in the middle of the element. These three shape functions do not satisfy the PUC. Figure 4 shows three different shape functions that satisfy the PUC. It is easy to show that both set represent the same spatial discretization. The shape functions of the Figure 4 are equivalent to the FE shape functions of two elements placed one after the other.

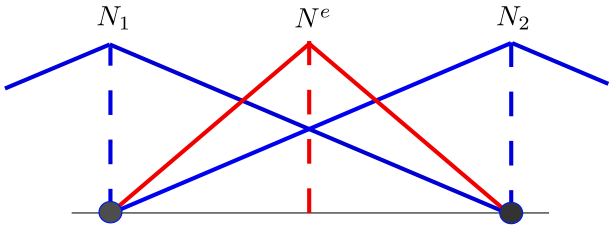

Fig. 3: Linear FE shape functions and enrichment for a kink non-satisfying the PUC

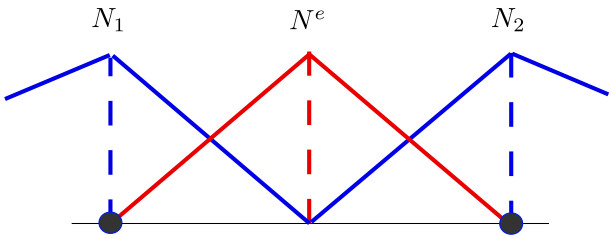

Fig. 4: Linear FE shape functions and enrichment for a kink satisfying the PUC

For problem with kinks and jumps the PUC solution may be represented as in Figure 5 in which two different shape functions are used for the enriched space.

In the same way, the enriched space for reproducing a kink or a jump inside a 2D triangle may be obtained subdividing the element in three sub-elements and using the standard FE shape functions of each sub-element. See subplot (a) on Figure 6 for the triangular subdivision and 6 subplot (b) and (c) for the shape functions for kinks, at left a perspective view and at right the level lines of the correspondent functions. In this case for N_1^e there is a region (one of the sub-elements coming from the partition) where this function is fully null.

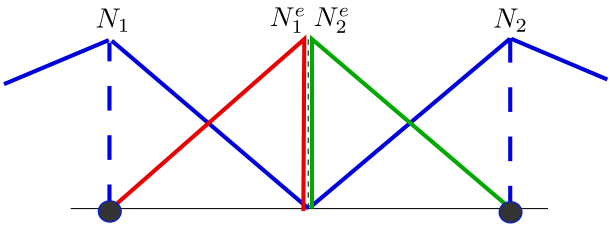

Fig. 5: Linear FE shape functions and enrichment for a kink + jump satisfying the PUC

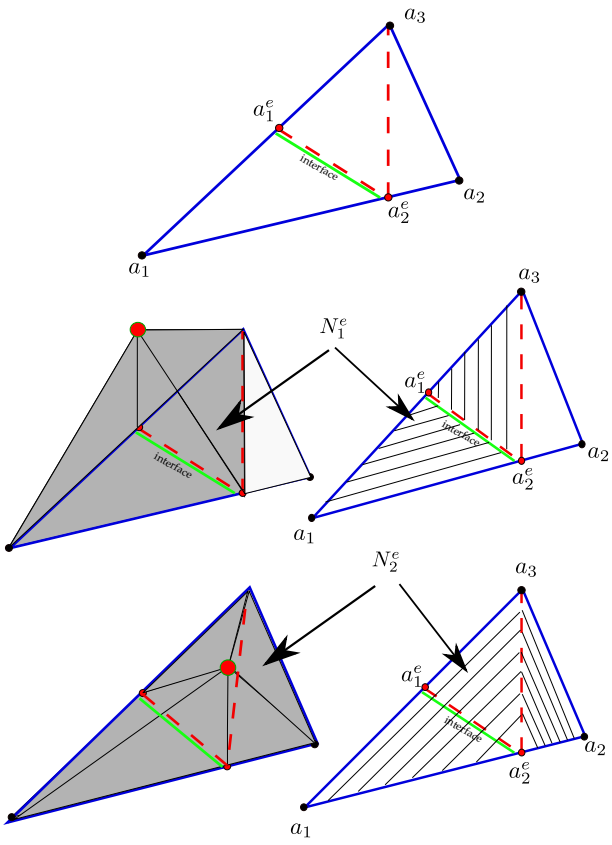

Fig. 6: (a) Triangular element subdivided in 3 sub-elements b) corresponding enriched shape functions for kinks satisfying the PUC

For the case of kinks + jumps the triangle is subdivided in the same way but duplicating the nodes at the internal interface (see Figure 7)

The procedure to obtain the final stiffness matrix of each element to be assembled in the global stiffness matrix is the following:

1. The extended stiffness matrix $\mathbf{K}_{ext}$ of each sub-element is assembled in one super-element of 5 nodes (for kinks) or 7 nodes (for kinks+jumps), with
$$\mathbf{K}_{ext} = \begin{bmatrix} \mathbf{K}^{nn} & \mathbf{K}^{ne} \\ \mathbf{K}^{en} & \mathbf{K}^{ee} \end{bmatrix}$$
where n and e are the subindexes of the original and added dofs of the element respectively.
2. The inter-element forces (18) are added just modifying $\mathbf{K}^{en}$ and $\mathbf{K}^{ee}$.

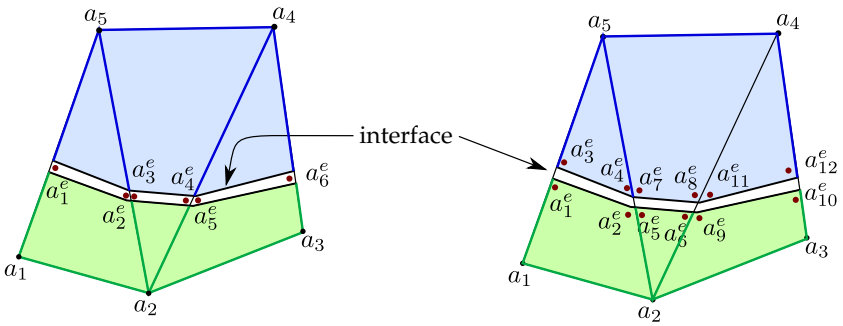

Fig. 7: Triangular elements are subdivided in 3 sub-elements and enriched DOFs are added. Left: Case for kinks. Right: Case for kinks + jumps.

3. The jumps conditions are introduced by 8 and 9
4. Finally the enriched DOF are eliminated by static condensation following

$$\mathbf{K} = \mathbf{K}^{nn} - \mathbf{K}^{ne} \left(\mathbf{K}^{ee}\right)^{-1} \mathbf{K}^{en}$$

being $\mathbf{K}$ a square matrix with the original size without enrichment. A similar procedure must be done for the r.h.s. vector.

In the case of three dimensional finite elements, the interface Γ_{int} is composed of planar facets which do not conform with the element faces. Again, the element can then be split into two sub-regions. As noticed in Fig. 8 for the three dimensional case, two possible situations have to be considered, since the reconstructed interface can be either a triangular or a quadrangular facet. In the first case, the tetrahedron is subdivided in 4 sub-elements, and in the second case, is divided in 6 sub-elements. Then, the enriched DOF's are eliminated by static condensation as usual.

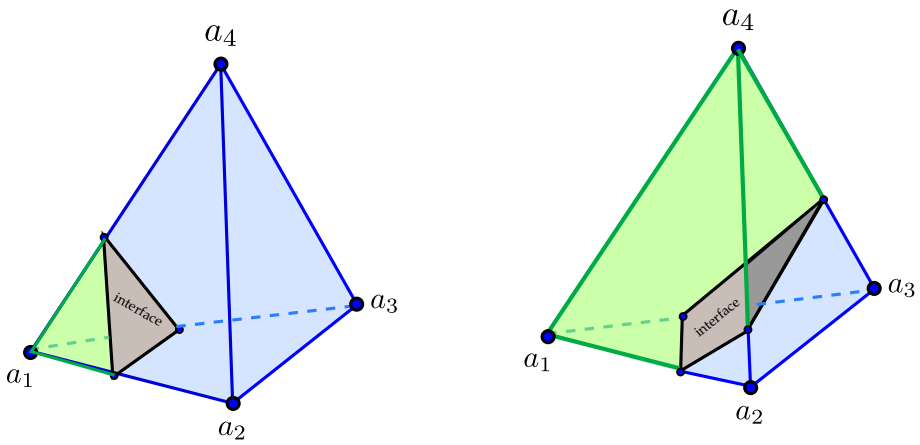

Fig. 8: Tetrahedron is subdivided in 4 or 6 sub-elements depending on cases presented at left and right images respectively.

6. Pathological cases

Two different cases of pathological problem will be referred next. One case is related to geometrical problems involved when the internal interface is near a node, very close to an interface or both. The other case is related to which decision must be taken when there are more than one result in the same position as currently occur in the elemental enriched space.

When an internal jump is coincident with a node or with an element interface, one of the sub-elements disappears or becomes very small, which can lead to numerical problems. One solution is to treat these elements in a different

way, avoiding one of the sub-elements and imposing a different constraint at the node or elemental interface level. All that casuistry is feasible but complicated of being implemented. Moreover, in three dimensions will appear new unsupported situations. A more simple solution consists of temporarily move some nodes a small quantity in order to avoid the singularity and back to its initial position once the stiffness matrix has been generated. A formal description of the employed strategy is presented in Algorithm 1, while Fig. 9 shows a graphical interpretation of the pathological case. Experimentally, employing a minimum distance node-interface $\epsilon \approx 0.005h$ where h is the element size of an unstructured mesh, the rate of modified nodes by time-step is low, i.e. around of 1% of nodes belonging to any element cut by interface are moved, what justifies the employment of this strategy.

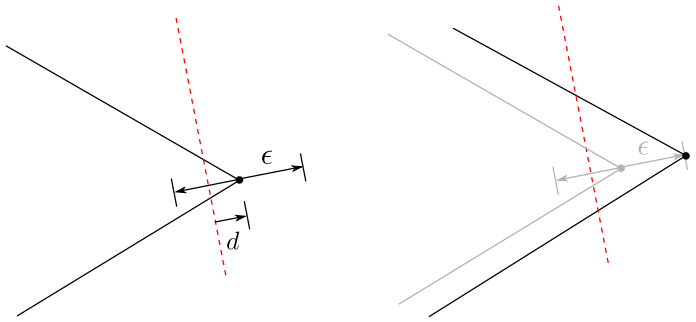

Fig. 9: Strategy to avoid unsupported cases. Left: initial situation with a node near than epsilon from the interface. Right: new position of the node far from the interface. This position will be reset after time-step.

Algorithm 1 - Time-Step using enrichment avoiding unsupported cases. d is the minimum Euclidean distance from node j at position $\mathbf{x}_j$ and the interface represented by the function λ. $\mathbf{n}$ is the interface normal.

1. store current nodal positions
2. update interface position λ
3. foreach node j
   (a) if $d(\mathbf{x}_j, \lambda) < \epsilon$
      i. $\mathbf{x}_j \leftarrow \mathbf{x}_j + sign(d(\mathbf{x}_j, \lambda))\ \epsilon\ \mathbf{n}$
      ii. update nodal states interpolating at new position.
4. solve differential equation system using enriched-FEM
5. restore original nodal positions

Other singularities occur in the case of jumps in the particular case where $\mathbf{J} = 0$ In this case, the stiffness matrix becomes singular. The explanation is very simple: when $\mathbf{J} = 0$ there is no connection between the triangular sub-element created on one side of the internal interface with the other two sub-elements (see Figure10). Indeed, the introduction of the inter-elemental forces makes that this triangular sub-element is only connected to the node indicated by a 1 in Figure 10. Besides, the condition $\mathbf{J} = 0$ means that the normal stresses are zero at the internal interface. Therefore, this sub-element can "rotate" about an imaginary axis perpendicular to the interface as shown in the Figure 10. To avoid this singularity the case $\mathbf{J} = 0$ is replaced by $\mathbf{J} = \epsilon$ where ϵ represents a relative small value (tolerance). A similar case to the previous one is when the jump $\| \mathbf{u} \|$ has a linear variation along the interface of an element. While the proposed linear element allows a linear variation of the jump, the imposition of the restrictions 8 and 9 at the elementary level, without "looking" what happens in the neighboring elements, restricts the jump variation to the constant case. To eliminate this difficulty the fact that a rotation of the triangular sub-element about an axis perpendicular to the interface passing through the node 1 does not absorb energy is taken into account. Thus, the triangular sub-element is rotated subsequently, as a post-process work, to suit the overall conditions of the problem.

Another singular case occurs when there is a strong variation of the stiffness coefficients between the two domains on both sides of the interface. This is a particular case because, as explained before, the triangular sub-element does not resist to a rotation. If the domain with the large stiffness coefficient is on the triangular sub-element, this means

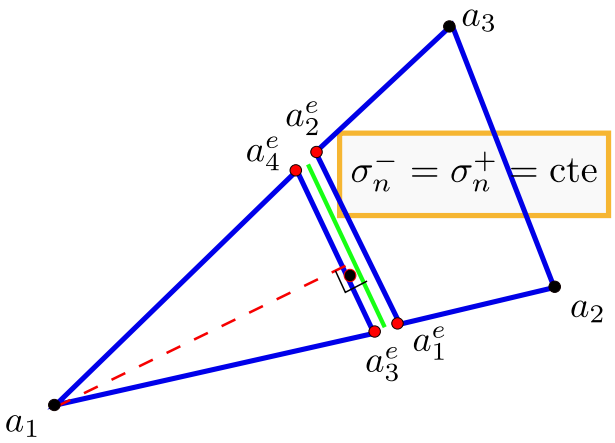

Fig. 10: Possibility of rotation of the triangular sub-element along an axis normal to the interface (in red dash line on the figure)

that the entire triangular element will have a small stiffness. For this reason, when this is the case, only the value of the unknown that are on the quadrangular sub-domain with the large stiffness coefficient are taken into account. See Figure 11.

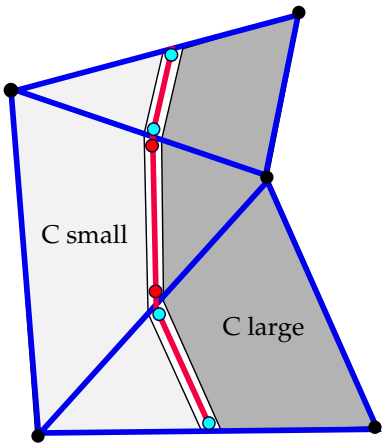

Fig. 11: Case with a strong variation of the stiffness coefficients. Only the value of the unknown that are on the quadrangular sub-domain with the large stiffness coefficient are taken into account. The values of the unknown marked in red are disregarded.

7. Numerical examples

The numerical examples chosen in this section are mainly thermal problems where the unknown function (the temperature) is a scalar function. The main objective is to highlight the errors and the accuracy of the elemental enrichment in this simpler context like the thermal conduction equation. The extension of this technique to vector unknown fields, like the displacement for solid mechanics or the velocities for fluid mechanics is straightforward.

7.1. One-dimensional kink: two materials

Figure 12 represents a one-dimensional thermal problem solved in a non-structured two-dimensional triangular mesh. There are two materials with different conductivity coefficients separated by an interface which splits the

domain in two parts. This strong variation of the conductivity coefficients introduces a kink in the temperature field at interface. An analytic solution can be found for this problem, being

$$T(x,y) = \begin{cases} \dfrac{2k_2}{k_1+k_2}y & y \leq 0.5 \\ \dfrac{2k_1}{k_1+k_2}(y-1)+1 & y > 0.5 \end{cases} \tag{26}$$

In order to solve the diffusion equation for the unknown T, $k_1 = 1$ y $k_2 = 10$ are chosen.

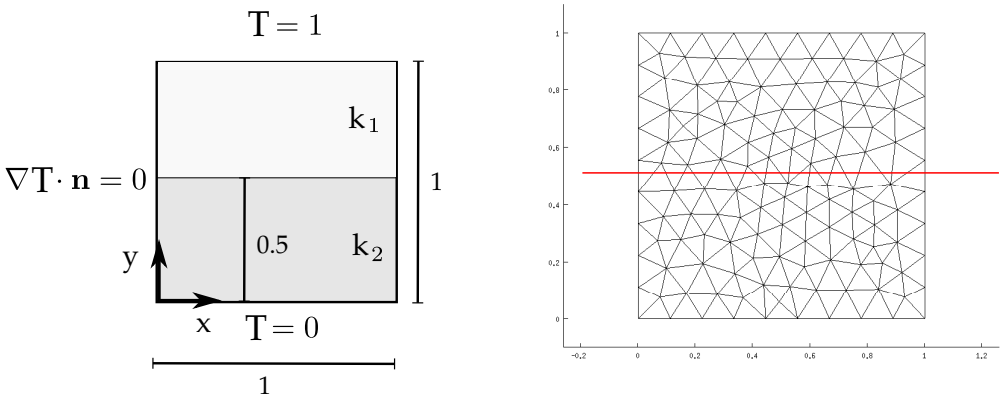

Fig. 12: One-dimensional kink by two materials. Configuration and mesh employed.

Figure 13a presents the analytic solution compared with three different numerical solutions obtained employing the proposed mesh. The solution with standard FEM, i.e. without enrichment, fails capturing the kink and estimates wrongly the temperature gradient which results in an unacceptable solution even in this simple case. As expected, using enrichment improves the kink capturing. However, the lack of the interelemental load term discussed previously leads to a solution which has some deficiencies specially in the region of small conductivity. That *variational crime* is clearly solved incorporating the mentioned term in the elemental assemble (solution with interelemental load). This difference is highlighted by Figure 13b where the value of the enriched degrees of freedom over the interface is presented. It is noticeable how including the interelemental load the solution obtained matches the analytic one while not employing it the solution is poor. Moreover, some enriched nodes at same physical point have different temperature values depending on the interface side where they are.

As seen in this first case, the only numerical strategy which guarantees an accurate solution when the mesh does not match the interface is employing enrichment with interelemental load.

7.2. One-dimensional kink: two materials and concentrated loads

Figure 14 represents another one-dimensional thermal problem solved in a two-dimensional triangular mesh. There are two materials with a big difference in their conductivity coefficients. Furthermore, there are two concentrated thermal loads near the interface between the two materials. The strong variation of the conductivity coefficients as well as the concentrated thermal loads introduce three kinks in the temperature field. This example has a very simple analytical solution with four piece-wise linear temperature variations.

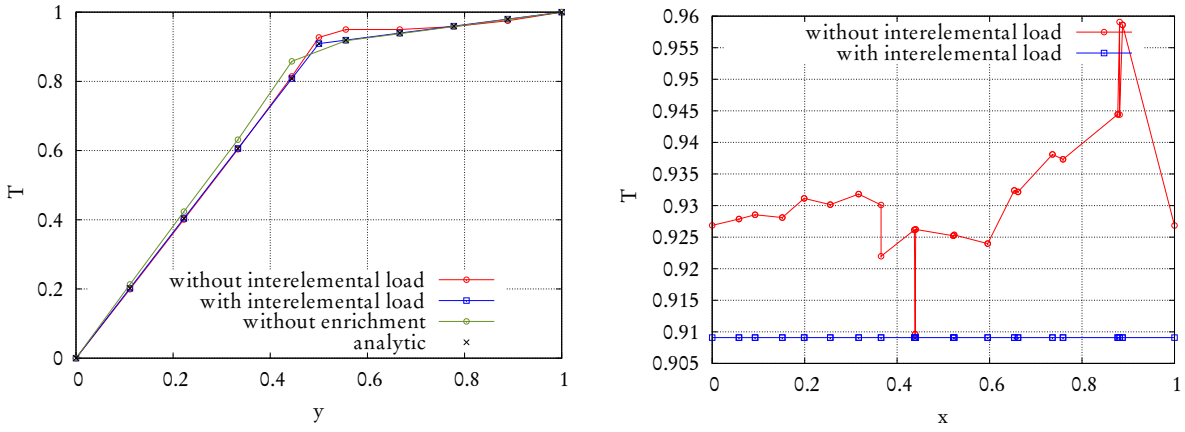

(a) $x = 1$ slice (b) $y = 0.5$ slice

Fig. 13: Solution over a vertical line and over the interface.

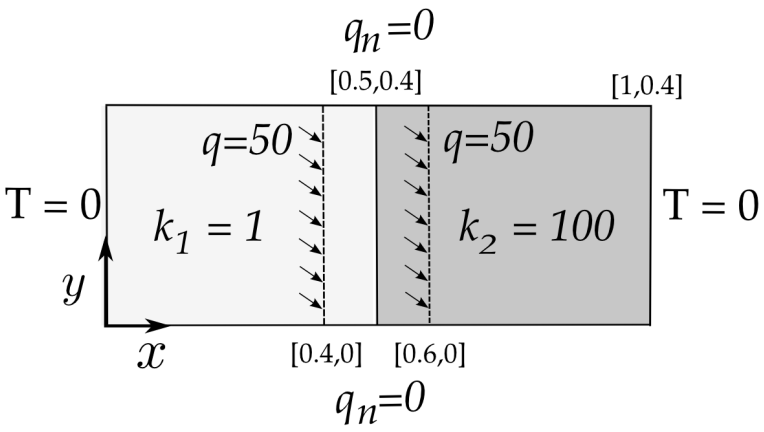

Fig. 14: One-dimensional problem with two different materials and concentrated loads. Problem definition.

Figure 15 shows the unstructured mesh used with the three lines showing the location where the elemental enrichment has been added.

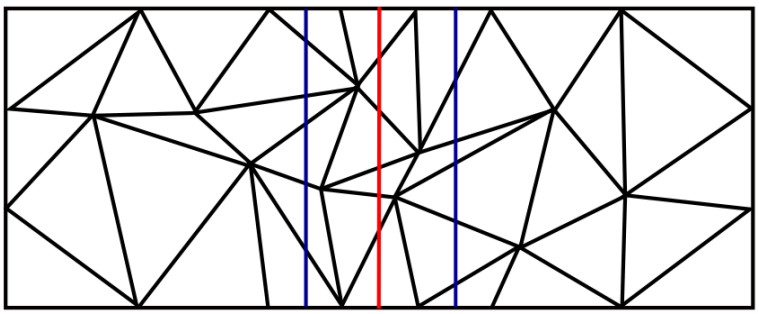

Fig. 15: One-dimensional problem with two different materials and concentrated loads. Mesh definition and lines where the elemental enrichment has been added: concentrated loads (in blue); change of conductivity (in red).

This is an interesting test to evaluate the importance in the usage of the enrichment space and the importance to the inter-elemental forces described in Eq. 18. Figure 16a, shows in black the solution of the elemental enrichment and the analytical solution superposed due to the very good agreement between them. In the same figure the solution without enrichment on the upper boundary (in green) and in the lower one (in blue) are shown. Errors greater than 100 % may be found in this example if no enrichment spaces are used. Furthermore, Figure 16b, shows the enriched solution obtained without the introduction of the inter-elemental forces. The solution is not constant if we move at different domain heights, which is inconsistent with the physics of the problem.

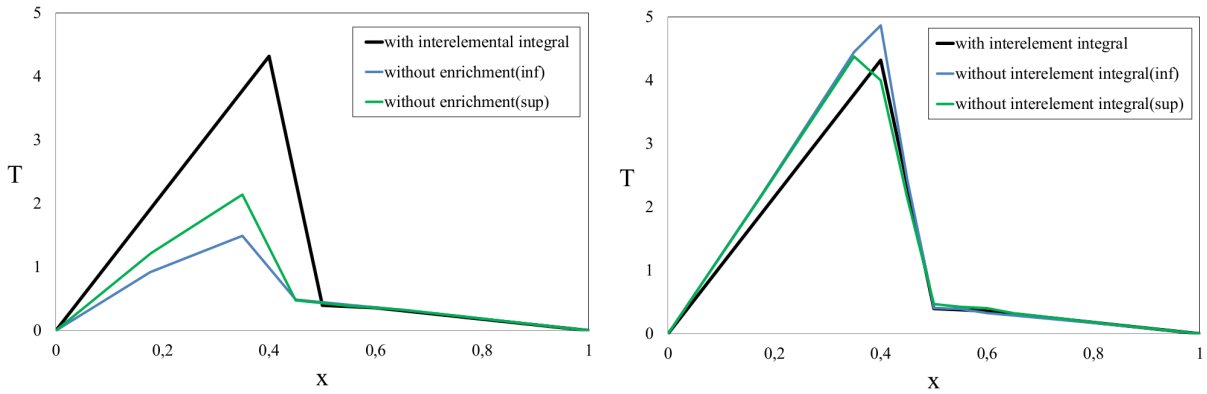

(a) (b)

Fig. 16: One-dimensional problem with two materials and concentrate loads. Fig. 16a: Comparison with the elemental enrichment and the solution without enrichment. Fig. 16b: Comparison with and without inter-elemental forces.

8. Two-dimensional Kink: two materials and concentrated loads

This example has been specially designed to ensure that the lack of connection that is obtained between two neighbor DOFs which have been condensed gives the maximum error. The boundary conditions and the unstructured mesh used is represented in Figure 17a and Figure 17b respectively.

For this two-dimensional problem there is not an analytic solution, but the results are compared with a matching fine mesh, where the interface with kinks are coincident with the interface of two elements. The result for the finest matching mesh is represented in Figure 17c. As we can see in the exact solution, this problem has a big curvature (high second derivative) of the temperature field in the same direction of the interface. This means a large variation perpendicular to the element side where there is not a good connection due to the condensation. For this reason, large errors are expected when using an elemental enriched space.

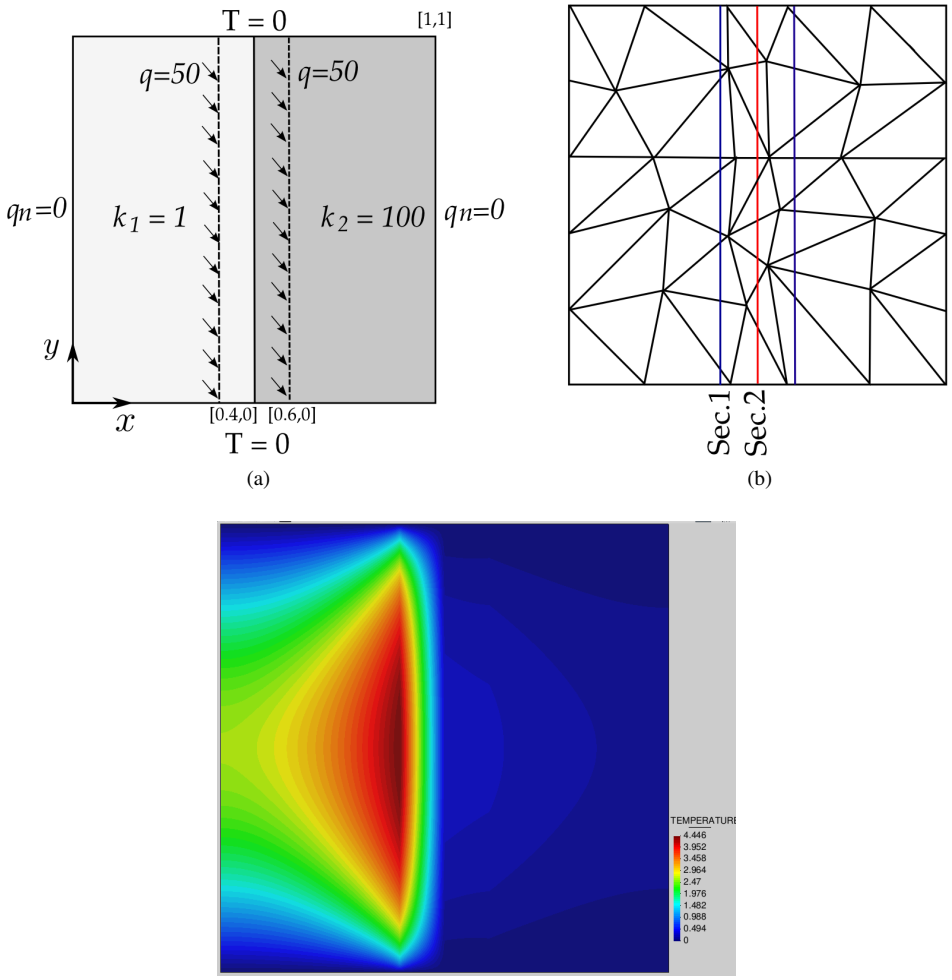

Fig. 17: Two materials and concentrate loads giving a big curvature of the unknown in the same direction of the interface. Fig. 17a: Problem definition. Fig 17b: Mesh used. 17c: Temperature distribution for the fine matching mesh.

Figure 18a shows the results on a horizontal line at the middle of the domain while 18b and 18c show the results on a vertical line at x=0.4 and x=0.5 respectively. The black line is showing the results on the unstructured mesh with the present enrichment and the dashed line the results with the matching mesh. Again in this example, despite of the large curvature of the results parallel to the interface, the enriched space is by far better than the results without enrichment with an error for this last one greater than 300 %. In this extreme example, the introduction of inter-elemental forces eliminates certain artificial jumps occurring between neighbor elements. See the green line in Figure 18b and 18c.

This green line shows artificial jumps in the results between two element when the inter-elemental forces are used. Although the continuity of the enriched functions are not ensured between two neighboring elements, the introduction of inter-elemental forces gives a continuous solution between neighbor elements while avoiding these loads for giving a nonphysical solution. While in this particular case, the use of the inter-elemental forces does not improve the overall accuracy of the results, the fact of obtaining a continuous numerical solution without artificial jumps is a great advantage. These results demonstrate once again the benefits of the inter-elemental forces.

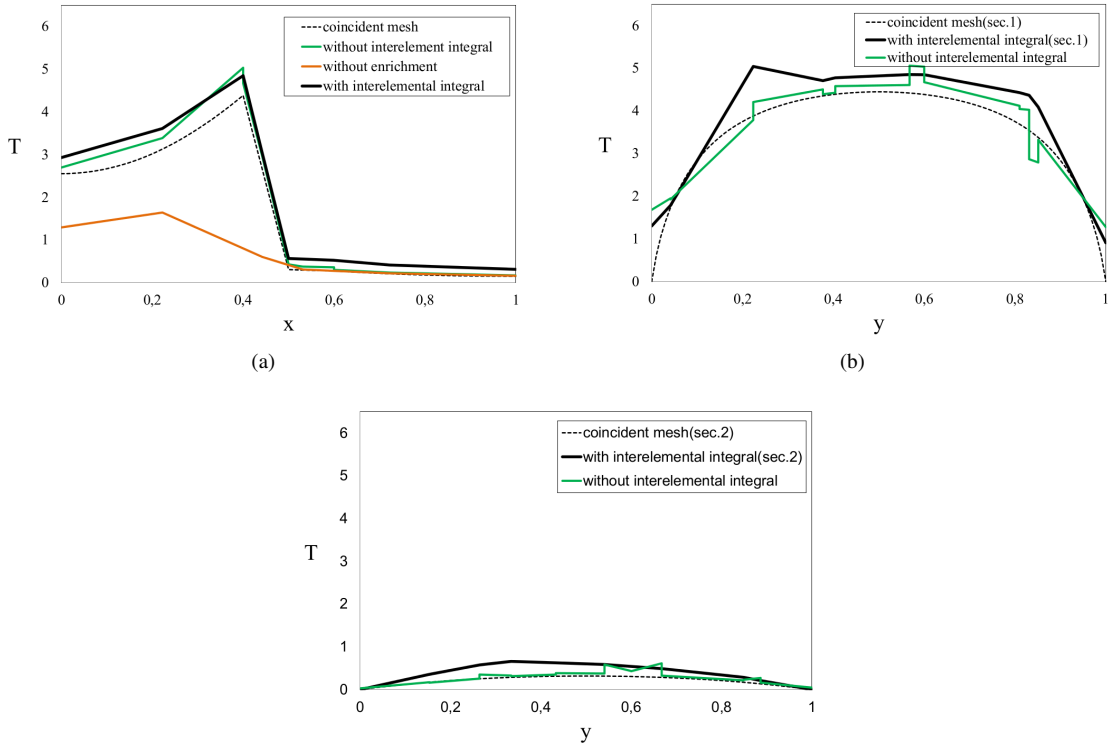

Fig. 18: Two materials and concentrate loads giving a big curvature of the unknown in the same direction of the interface. Fig. 18a Results on a horizontal line in the middle. Fig. 18b: Results on a vertical line in x=0.4. Fig. 18c: Results on a vertical line in x=0.5.

9. One-dimensional jump for different coefficients

The following example is the first one with a jump in the unknown field. A jump in the temperature in a thermal problem may be considered when there are two domains in contact but supposing that there is another material in between the two domains very mince with a different conductivity. It is, for instance, the case of the contact between two metals but with a roughened contact surface leaving some air gap between them. The amount of conductivity between the two domains is regulated by the coefficient **J** described in Eq. 9.

Figure 19 describes the boundary conditions and the mesh used to solve a two-dimensional version with triangular finite elements of a simple one-dimensional problem.

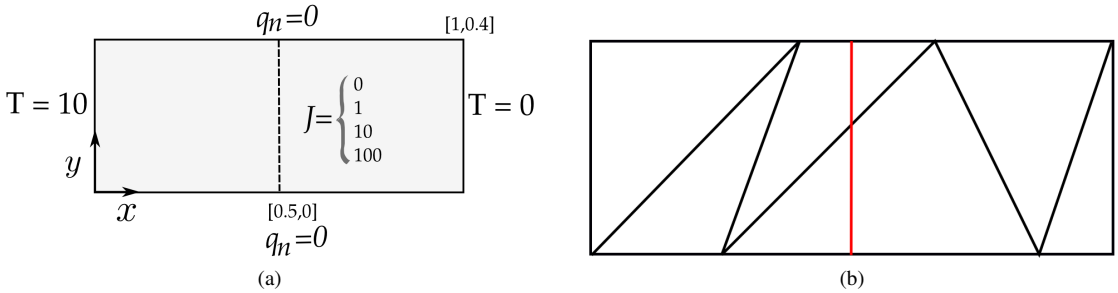

Fig. 19: One-dimensional problem with a jump. a) Boundary conditions; b) mesh used.

As in the one-dimensional problem solved previously for kinks, this example is interesting to show the importance

to introduce the inter-elemental forces also in problem with jumps. Figure 20 shows the temperature results for different values of the **J** coefficient at left. In all the cases, the enrichment proposed with the inter-elemental forces gives the exact result in any horizontal line. However, when the inter-elemental forces are not included, the results are not coincident with the analytic ones and they are not the same at different horizontal lines. Fig. 20b shows the case of $\mathbf{J} = 1$.

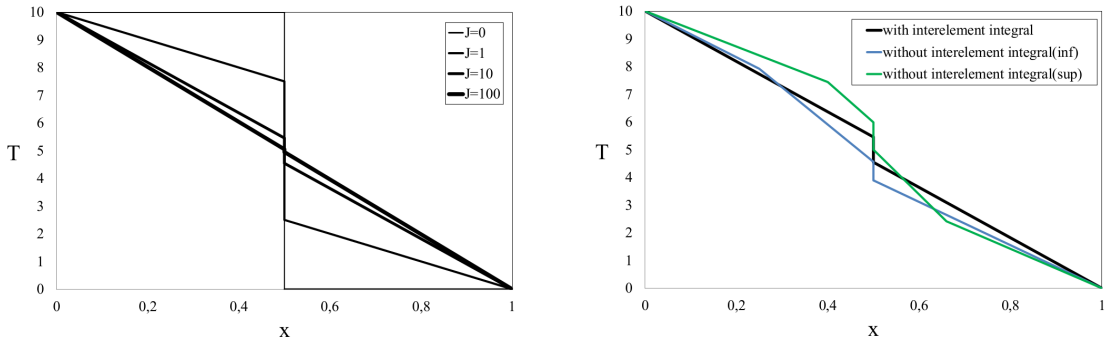

(a) (b)

Fig. 20: One-dimensional problem with a jump. Fig. 20a: Temperature distribution for different J values. Fig. 20b: Temperature distribution for J=1 and comparison with the results without inter-elemental forces

10. Jumps + Kinks: two materials with J=1

This example was thought to test the possibility of the new enrichment space to approximate problem where the jump is variable along the interface. Figure 21a shows the boundary condition of the problem, which in fact is like a rotation of the unknown function on the right wall while the left wall remain constant. The imposition of a jump with $\mathbf{J} = 1$ in the vertical middle will suppose to have a positive jump on the upper bound and a negative one on the bottom.

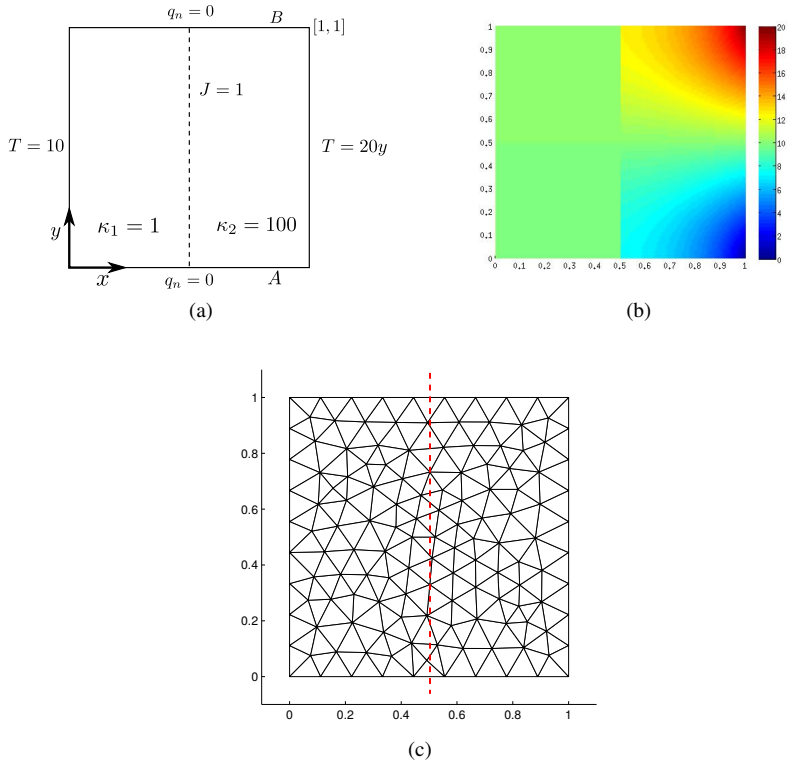

Fig. 21: Two-dimensional problem with a variable jump. Fig. 21a: Boundary Conditions. Fig. 21b: Solution with a fine and matching mesh. Fig. 21c: Coarse mesh used with the enriched space.

As there is not any analytic solution of this problem, the results will be compared with the solution obtained with a fine mesh coincident with the interface. In Fig. 21b the solution with the fine mesh is presented and Fig. 21c shows the unstructured coarse mesh used to solve the problem with the enriched space. Fig. 22a shows the results on both sides of the interface for the fine mesh and the coarse enriched mesh. In Figure 22b the results on the top line and the bottom line are drawn. It is interesting to note the accuracy of the results and the lack of artificial jumps of the function from one element to another even though the continuity of the function is not imposed between two neighboring elements.

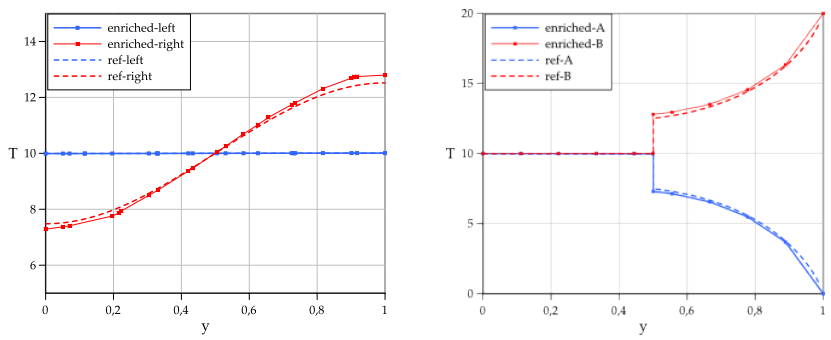

Fig. 22: Two-dimensional problem with a variable jump. (a): Unknown function along both side of the interface for the fine mesh and the coarse enriched mesh. (b): Unknown function on the top and the bottom line for both meshes

This example is also employed to introduce the convergence order of the error. The main idea is measuring the root mean square (RMS) between the values of the numerical results with enrichment, with different mesh refinements, and the reference solution. The RMS is calculated at the critical region of the problem, i.e. the values sampled over lines at both sides of the interface. Table 1 presents the results where a linear convergence order can be detected. The coarsest mesh of element size h is the same as presented in Fig. 21c. Successive meshes are generated requiring a smaller h, but not linked to the reference one.

	RMS left	RMS right
h	0.0519	0.0693
h/2	0.0245	0.0445
h/4	0.0160	0.0285
h/8	0.0107	0.0141

Table 1: RMS of the difference between solution with enrichment with different meshes and the reference solution with a fine coincident mesh.

11. Jumps + Kinks with variable J

This example is very similar to the typical cracks problems, where there is an interface with a crack and the remaining domain keeps continuous. The crack will be represented by imposing a very small value of the coefficient J while the remaining domain will be without any enrichment or including an enrichment with a large value of the coefficient J, as presented in Fig. 23a. The solution obtained with the coarse mesh with enrichment using the same mesh shown in Figure 21c is compared with the solution obtained with a fine and matching mesh shown in Figure 23b.

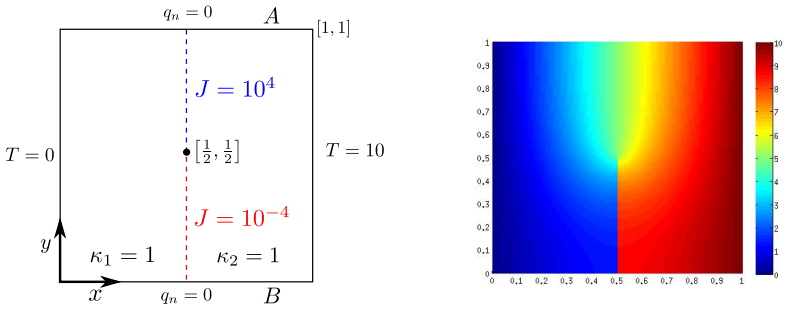

(a) (b)

Fig. 23: Two-dimensional problem with a crack. Fig. 23a: Boundary Conditions. Fig. 23b: Solution with a fine and matching mesh.

This example is interesting because the magnitude of the crack is variable inside each element, showing the versatility of the proposed enriched element. Although there is a small oscillation of the results at the point where the crack starts, Fig. 24a, the agreement of the results with the exact solution obtained with the fine mesh is admirable even though it has been obtained with a coarse mesh.

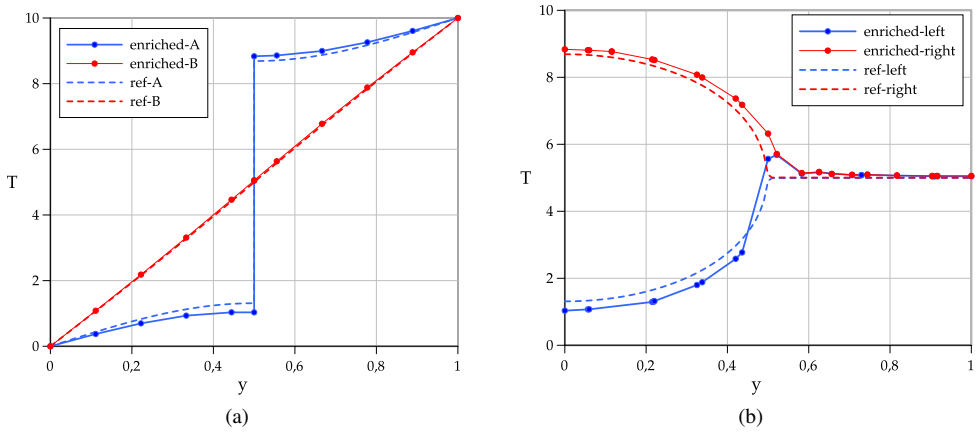

Fig. 24: Two-dimensional problem with a crack. Fig. 24a: Unknown function on both sides of the discontinuity compared with the fine matching mesh. Fig. 24b: Unknown function on the top and bottom line.

12. Moving jumps in homogeneous domains

The following examples have been thought to show the capability of the enriched space proposed to move discontinuous fields through coarse fixed meshes. It is interesting to note again that all the results not only use the same mesh, but they use exactly the same matrix graph, this means that the solution matrix has exactly the same DOFs although the interface move its position. The first one is represented in Fig. 25. It is a constant flux field with T=0 on the left boundary and T=10 on the right one, that include an adiabatic wall in the middle which rotates around its own centre. The coarse mesh used with the enriched space is the same as presented in Fig. 21c. The temperature distribution for different position of the adiabatic wall is shown in Fig. 26.

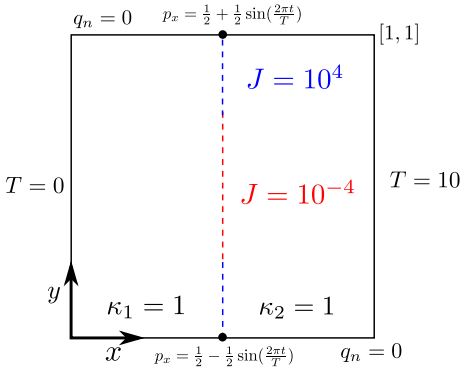

Fig. 25: Flujo constante con una chapa adiabtica rotante.

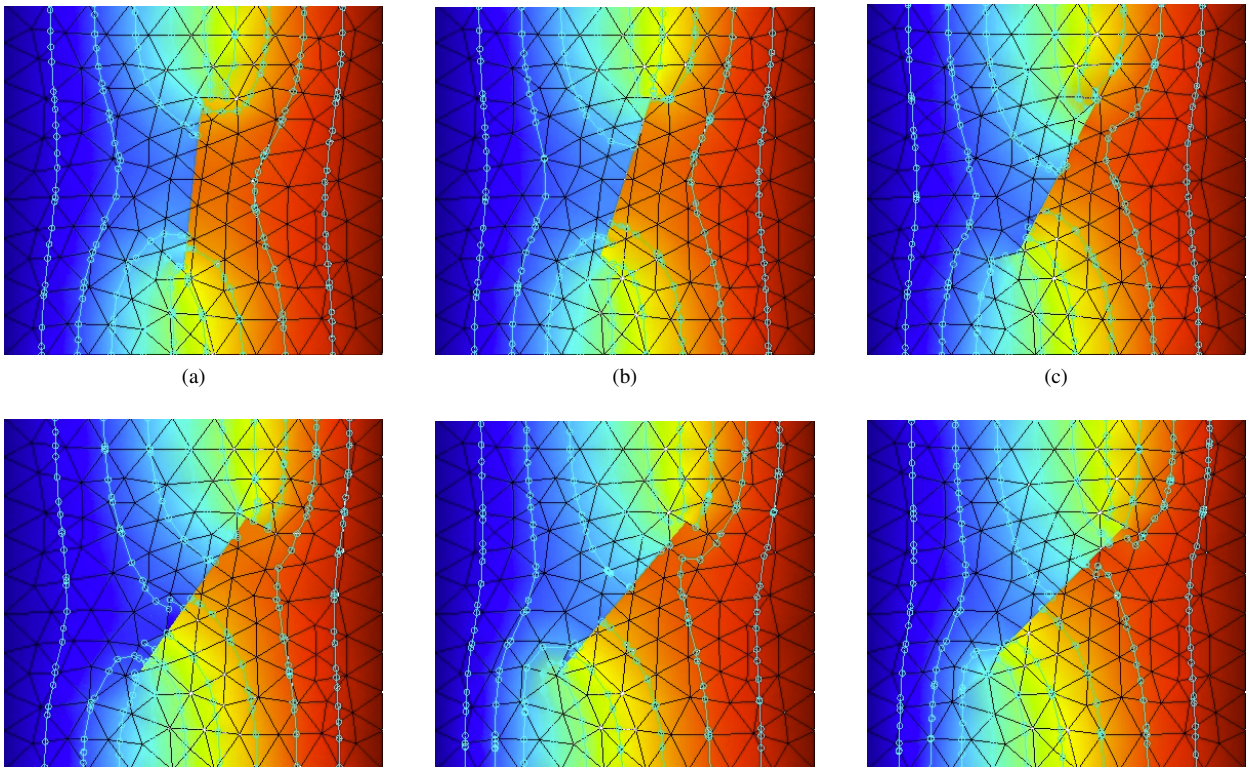

Fig. 26: Constant flux with an adiabatic wall rotating. Temperature distribution for different position of the adiabatic wall.

Another problem, that is also difficult to solve with a fixed mesh, is described in Fig. 27.

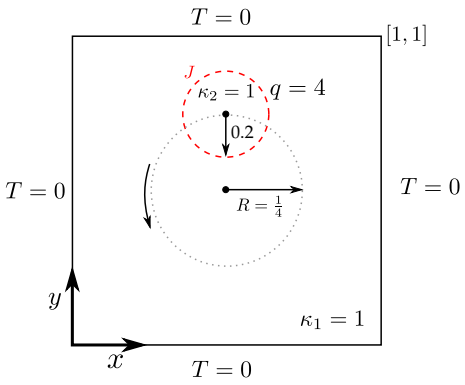

Fig. 27: Circle with a concentrated load moving freely around a fixed mesh. Problem definition.

There is now a thermal load concentrated around a circle and the entire circle domain is adiabatic with respect to the remaining part. The thermal load and the adiabatic condition introduce a sharp discontinuity in the temperature field. Furthermore, the circle moves freely around the fixed mesh. We have used the same coarse mesh of the previous example. The temperature distribution at different positions is shown in Figure 28 A cut of temperature distribution may be seen in Figure 29. The ability of the proposal presented in this paper to represent jumps of any shape and any position on the mesh is well demonstrated with this example. It can be noticed that this type of situation usually

appears in microfluidics: the pressure field inside and outside a bubble or a drop has a sharp discontinuity due to surface tension. The capability of the enrichment strategy shows very optimistic results compared with the majority of the surface tension treatments over coarse meshes, which are not able to reproduce the pressure jump even when the analytic curvature is employed.

The last test is similar to the example previously shown, but instead of imposing the adiabatic condition around the cylinder ($J = 0.01$) a coefficient J=10 is introduced. The example can be seen as the temperature field around an immersed solid. Due to the fact that the boundary layer cannot be captured with this coarse mesh, the idea is to calibrate J in order to model the transition from the solid temperature to the environment. Figure 30 shows the temperature distribution for different position of the cylinder and Figure 31 the temperature result on a horizontal line. It is interesting to see that when the cylinder contour is near a boundary domain, where the temperature is imposed to zero, the temperature jump on the cylinder becomes sharper while a more diffusive solution is obtained when the cylinder contour is far from the domain boundary.

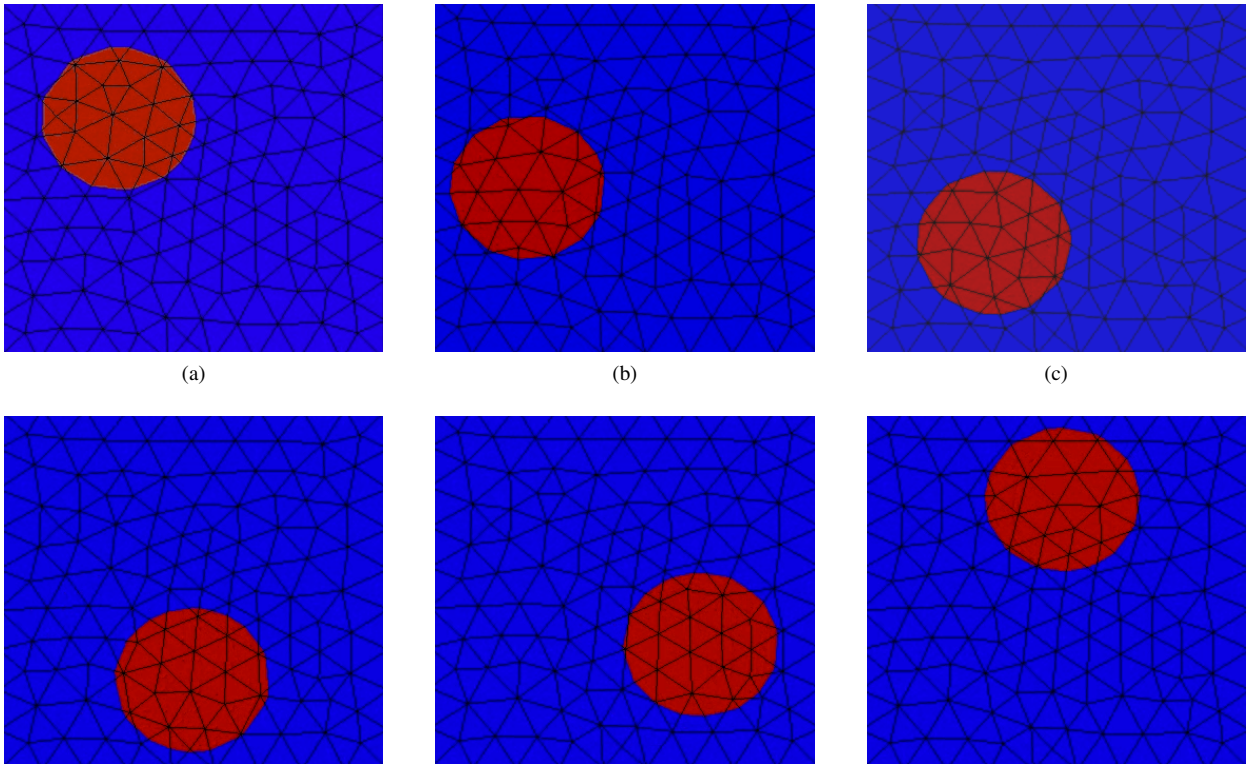

Fig. 28: Circle with a concentrated load moving freely around a fixed mesh. Temperature distribution for different position of the cylinder

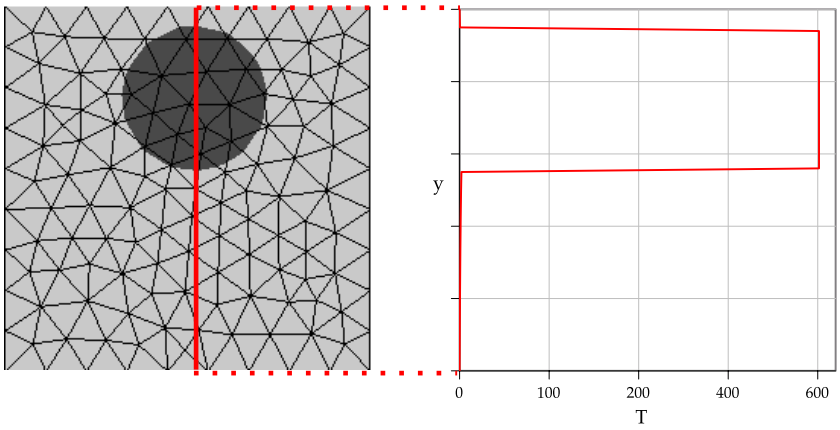

Fig. 29: Circle with a concentrated load moving freely around a fixed mesh.Temperature distribution along a vertical line at the end of the lap.

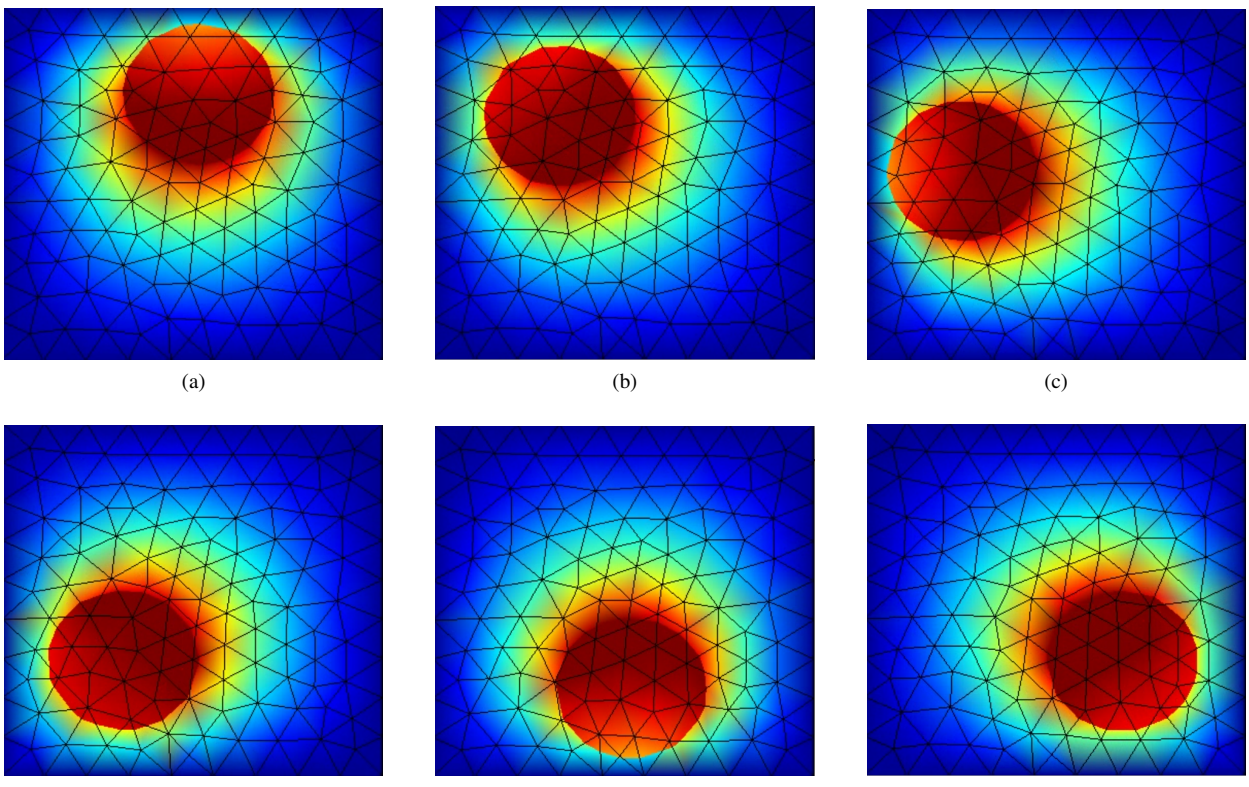

Fig. 30: Circle with a concentrated load moving freely around a fixed mesh. J=10. Temperature distribution for different position of the cylinder

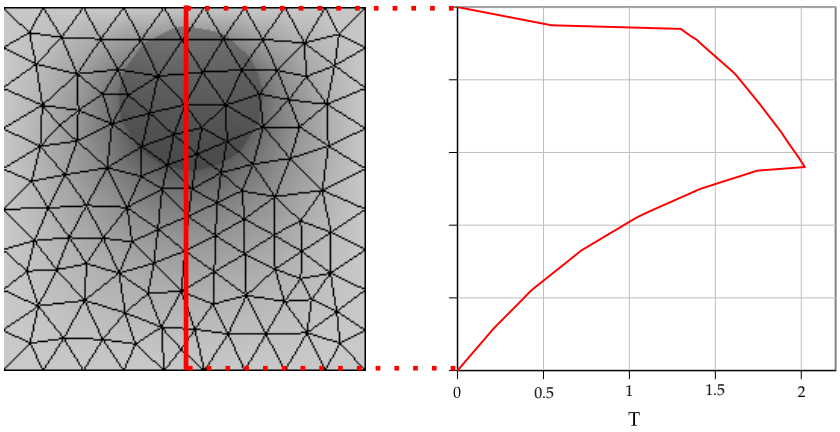

Fig. 31: Circle with a concentrated load moving freely around a fixed mesh. J=10. Temperature distribution along a vertical line.

13. Conclusions

An enrichment space for the treatment of both: jumps or kinks have been presented. The new space allows for a linear variation of the kink or the jump inside each element and the new degrees of freedom introduced may be condensed at elemental level having all features of an elemental enrichment (EFEM). In order to decrease considerably the variational crimes introduced when an elemental enrichment is used for an unknown fields that have second derivative in space, like displacements, velocities or temperature in the conservation equations, a contour integral has been added at each element boundary. These contour integrals can be interpreted as a "do nothing" boundary condition on the elemental boundaries or the use of weighting functions that ensure convergence of the approach in the sense proposed by J.C. Simo [2] for the enriched spaces.

The implementation of this new element in any existing finite element code is extremely easy in both two and three spatial dimensions, because the new shape functions are based on the usual C^0 FEM shape functions for triangles or tetrahedral and, once statically condensed the internal DOFs, the resulting element has exactly the same DOFs as the non-enriched FE. This element has been specially thought for problem where there are moving internal interfaces, because those are the cases where the elemental enrichment is more efficient presenting an important reduction of the computing time compared with nodal enrichment.

A series of numerical tests for scalar unknowns (temperature) were presented to illustrate the performance of the elemental enriched space. In the examples, the importance of adding the contour integral around each element has been proved given in this case the exact solution when the enriched space is in the same space of the solution. The importance to have a linear variation of the jump has been shown in the crack simulation, where with a very coarse mesh an accurate representation of a crack problem has been achieved. Finally, in problems with moving interfaces, the incredible versatility for solving different problems, all with exactly the same fixed mesh, has been shown.

Although in this paper only problems with scalar unknowns as temperature has been tested, the authors consider that the problem of enrichment spaces is exactly the same for vector unknowns and therefore, hope that these ideas will be useful to other authors who need to solve problems in the field of solid and fluid mechanics with large moving discontinuities.

14. Acknowledgments

The authors thank Xavier Oliver from the Polytechnic University of Catalunya and Gustavo Buscaglia from Sao Paulo University for the permanent discussions about this subject and for supporting and clarifying many aspect of this research. This work was supported by ERC-Proof of Concept Grant-2014 FORECAST from the European Research Council and the COMETAD project of the National RTD Plan (ref. MAT2014-60435-C2-1-R) from the *Ministerio de Economa y Competitividad* of Spain. Juan Gimenez and Norberto Nigro wish to acknowledge CONICET, Universidad

Nacional del Litoral and ANPCyT for their financial support through grants PIP-2012 GI 11220110100331, CAI+D 2011 501 201101 00435 LI and PICT-2013 0830.

References

[1] Coppola-Owen H. and Codina R. A free surface finite element model for low froude number mould filling problems on fixed meshes. Int. J. Numer. Meth. Fluids, 66:833851, 2011.

[2] Simo J. and Rifai M. A class of mixed assumed strain methods and the method of incompatible modes. Int. J. Num. Meth. Eng., 29:1595–1638, 1990.

[3] Sommerfeld M, van Wachem B, and Oliemans R. Best Practice Guidelines. ERCOFTAC, Special Interest Group on Dispersed Turbulent Multi-Phase Flow. ERCOFTAC, 2007.

[4] Hughes T., Liu W., and Zimmermann T. Lagrangianeulerian finite element formulation for incompressible viscous flows. Computer Methods in Applied Mechanics and Engineering, 29:329349, 1981.

[5] Donea J., Huerta A., Ponthot J., and Rodrguez Ferran A. Encyclopedia of Computational Mechanics, Vol.1: Arbitrary LagrangianEulerian methods. Stein E. and de Borst R. and Hughes T. (eds.) John Wiley & Sons, New York, 2004.

[6] Hirt C., Amsden A., and Cook J. An arbitrary lagrangianeulerian computing method for all flow speeds. Journal of Computational Physics, 14:227253, 1974.

[7] Cruchaga M., Celentano D., and Tezduyar T. A moving lagrangian interface technique for flow computations over fixed meshes. Computer Methods in Applied Mechanics and Engineering,, 11:525–543, 2001.

[8] Dettmer W., Saksono P., and Peric D. On a finite element formulation for incompressible newtonian fluid flows on moving domains in the presence of surface tension. Communications in Numerical Methods in Engineering, 19:659–668, 2003.

[9] Baiges J., Codina R., and Coppola-Owen H. The fixed-mesh ale approach for the numerical simulation of floating solids. International Journal for Numerical Methods in Fluids, 67(8):10041023, 2011.

[10] Idelsohn S., Oñate E., and Del Pin F. The particle finite element method a powerful tool to solve incompressible flows with free-surfaces and breaking waves. International Journal of Numerical Methods, 61:964–989, 2004.

[11] Idelsohn S., Mier-Torrecilla M., and Oñate E. Multi-fluid flows with the particle finite element method. Comput. Meth. Appl. Mech. Engrg., 198:2750–2767, 2009.

[12] Mier-Torrecilla M., Idelsohn S., and Oñate E. Advances in the simulation of multi-fluid flows with the particle finite element method. application to bubble dynamics. International Journal for Numerical Methods in Fluids, 67(11):1516–1539, 2011.

[13] Idelsohn S., Mier-Torrecilla M., Nigro N., and Oñate E. On the analysis of heterogeneous fluids with jumps in the viscosity using a discontinuous pressure field. Computational Mechanics, 46(1):115124, 2010.

[14] Unverdi S. and Tryggvason G. A front-tracking method for viscous, incompressible, multi-fluid flows. Journal of Computational Physics, 100:1992, 25-37.

[15] Gueyffier D., Lie J., Nadim A., Scardovelli R., and Zaleski S. Volume-of-fluid interface tracking with smoothed surface stress methods for three-dimensional flows. Journal of Computational Physics, 152:423456, 1999.

[16] Popinet S. and Zaleski S. A front-tracking algorithm for accurate representation of surface tension. International Journal for Numerical Methods in Fluids, 30:775793, 1999.

[17] Hirt C. and Nichols B. Volume of fluid (vof) method for the dynamics of free boundaries. J. Comput. Phys, 39(1):201–225, 1981.

[18] Kothe D., Rider W., Mosso S., Brock J., and Hochstein J. Volume tracking of interfaces having surface tension in two and three dimensions. Technical Report Technical Report AIAA 96-0859, AIAA, 1996.

[19] Cummins S., Francois M., and Kothe D. Estimating curvature from volume fraction. Computers and Structures, 83:425434, 2005.

[20] Adalsteinsson D. and Sethian J. A fast level set method for propagating interfaces. Journal of Computational Physics, 118:269277, 1995.

[21] Sethian J. Evolution, implementation, and application of level set and fast marching methods for advancing fronts. Journal of Computational Physics, 169:503–555, 2001.

[22] S.J. Osher and R.P. Fedkiw. Level set methods: an overview and some recent results. Journal of Computational Physics, 169:463 – 502, 2001.

[23] Guermond J. and Quartapelle L. A projection fem for variable density incompressible flows. Journal of Computational Physics, 165:167–188, 2000.

[24] Shu C. and Osher S. Efficient implementation of essentially non-oscillatory shock-capturing schemes. Journal of Computational Physics, 77:439471, 1988.

[25] Jiang G. and Peng D. Weighted eno schemes for hamiltonjacobi quations. SIAM Journal on Scientific Computing, 21:21262144, 2000.

[26] Sweby P. High resolution schemes using flux limiters for hyperbolic conservation laws. SIAM Journal on Numerical Analysis, 21:9951011, 1984.

[27] Enright D., Fedkiw R., Ferziger J., and Mitchell I. A hybrid particle level set method for improved interface capturing. Journal of Computational Physics, 183(1):83 – 116, 2002.

[28] Marchandise E., Remacle J., and Chevaugeon N. A quadrature-free discontinuous galerkin method for the level set equation. Journal of Computational Physics, 212:338357, 2006.

[29] Di Pietro D., Lo Forte S., and Parolini N. Mass preserving finite element implementations of the level set method. Applied Numerical Mathematics, 56:11791195, 2006.

[30] Enright D., Losasso F., and Fedkiw R. A fast and accurate semi-lagrangian particle level set method. Computers and Structures, 83:479490, 2005.

[31] Strain J. Semi lagrangian methods for level set equations. Journal of Computational Physics, 151:498533, 1999.

[32] Strain J. Tree methods for moving interfaces. Journal of Computational Physics, 151:616648, 1999.

[33] Brackbill J., Kothe D., and Zemach C. A continuum method for modeling surface tension. Journal of Computational Physics, 100:335–354, 1992.
[34] Löhner R., Yang C., and Oñate E. On the simulation of flows with violent free surface motion. Computer Methods in Applied Mechanics and Engineering, 195:55975620, 2006.
[35] Carrica P., Wilson R., and Stern F. An unsteady single-phase level set method for viscous free surface flows. International Journal of Numerical Methods in Fluids, 53:229–256, 2007.
[36] Ganesan S., Matthies G., and Tobiska L. On spurious velocities in incompressible flow problems with interfaces. Computer Methods in Applied Mechanics and Engineering, 196:1193–1202, 2007.
[37] Ausas R., Sousa F., and Buscaglia G. An improved finite element space for discontinuous pressures. Computer Methods in Applied Mechanics and Engineering, 199:10191031, 2010.
[38] Buscaglia G. and Ausas R. Variational formulations for surface tension, capillarity and wetting. Computer Methods in Applied Mechanics and Engineering, 200(45-46):30113025, 2011.
[39] P. D. Minev, T. Chen, and K. Nandakumar. A finite element technique for multifluid incompressible flow using eulerian grids. Journal of Computational Physics, 187:255–273, 2003.
[40] Chessa J. and Belytschko T. An extended finite element method for two-phase fluids. Journal of Applied Mechanics, 70:1017, 2003.
[41] Belytschko T., Moës N., Usui S., and Parimi C. Arbitrary discontinuities in finite elements. International Journal for Numerical Methods in Engineering, 50:9931013, 2001.
[42] Strouboulis T., Babuška I., and Copps K. The design and analysis of the generalized finite element method. Computer Methods in Applied Mechanics and Engineering, 181:43–69, 2000.
[43] Duarte C., Babuška I., and Oden J. Generalized finite element methods for three-dimensional structural mechanics problems. "Computers and Structures", 77(2):215232, 2000.
[44] Gross S. and Reusken A. An extended pressure finite element space for two-phase incompressible flows with surface tension. Journal of Computational Physics, 224:4058, 2007.
[45] Henning Sauerland and Thomas-Peter Fries. The stable XFEM for two-phase flows. Computers & Fluids, 87:41 – 49, 2013.
[46] John W. Barrett, Harald Garcke, and Robert Nürnberg. A stable parametric finite element discretization of two-phase navier–stokes flow. Journal of Scientific Computing, 63(1):78–117, 2015.
[47] Fries T. and Belytschko T. The extended/generalized finite element method: An overview of the method and its applications. Int. J. Numer. Meth. Engng., 84:253–304, 2010.
[48] Coppola-Owen H. and Codina R. Improving eulerian two-phase on finite element approximation with discontinuous gradient pressure shape functions. International Journal for Numerical Methods in Fluids, 49:1287 – 1304, 2005.
[49] Gimenez J. and González L. An extended validation of the last generation of particle finite element method for free surface flows. Journal of Computational Physics, 284(0):186 – 205, 2015.
[50] Ausas R., Buscaglia G., and Idelsohn S. A new enrichment space for the treatment of discontinuous pressures in multi-fluid flows. International Journal for Numerical Methods in Fluids, 70(7):829–850, 2012.
[51] Oliver J., Huespe A., and Samaniego E. A study on finite elements for capturing strong discontinuities. Int. J. Num. Meth. Engrg., 56:2135–2161, 2003.
[52] Oliver J., Huespe A., and Sánchez P. A comparative study on finite elements for capturing strong discontinuities: e-fem vs x-fem. Comput. Methods Appl. Mech. Engrg., 195:4732–4752, 2006.
[53] Linder C. and Armero F. Finite elements with embedded strong-discontinuities for the modeling of failure of solids. International Journal for Numerical Methods Engineering, 72:1391–1433, 2007.
[54] Papanastasiou T., Malamataris N., and Ellwood K. A new outflow boundary condition. International Journal for Numerical Methods in Fluids, 14:587608, 1992.
[55] Behr M. On the application of slip boundary conditions on curved boundaries. International Journal for Numerical Methods in Fluids, 45:4351, 2004.